DNA 2925Z
AA-R-7134-2283
September 1972

EQUATIONS OF STATE FOR GEOLOGIC MATERIALS

S. H. Schuster, Applied Theory Inc.
J. Isenberg, Agbabian Associates

Prepared for

DEFENSE NUCLEAR AGENCY
Washington, D.C.

AGBABIAN ASSOCIATES
Los Angeles, California

Contract No. DNA001-72-C-0045

UNCLASSIFIED
Security Classification

DOCUMENT CONTROL DATA - R&D

(Security classification of title, body of abstract and indexing annotation must be entered when the overall report is classified)

1. ORIGINATING ACTIVITY (Corporate author)	2a. REPORT SECURITY CLASSIFICATION
Agbabian Associates 8939 So. Sepulveda Boulevard Los Angeles, California 90045	UNCLASSIFIED 2b. GROUP

3. REPORT TITLE

Equations of State for Geologic Media

4. DESCRIPTIVE NOTES (Type of report and inclusive dates)

Final Report November 1971 through May 1972

5. AUTHOR(S) (Last name, first name, initial)

Schuster, Sheldon H. (Applied Theory, Inc.)
Isenberg, J. (Agbabian Associates)

6. REPORT DATE	7a. TOTAL NO. OF PAGES	7b. NO. OF REFS
June 1972	53	67

8a. CONTRACT OR GRANT NO.	9a. ORIGINATOR'S REPORT NUMBER(S)
~~DAGA01-71-C-0093-P00001~~ b. PROJECT NO. DNA001-72-C-0045 NWER Code XAXS c. Task and Subtask: B047 d. Work Unit 08	9b. OTHER REPORT NO(S) (Any other numbers that may be assigned this report) DNA 2925Z

10. AVAILABILITY/LIMITATION NOTICES

Approved for public release;
distribution unlimited.

11. SUPPLEMENTARY NOTES	12. SPONSORING MILITARY ACTIVITY
	Director, Defense Nuclear Agency Washington, D.C. 20305

13. ABSTRACT

This report considers data and mathematical models for geological materials subjected to shock loading. The high pressure equation of state is a modification of the Tillotson form. The modifications include accounting for energy due to vaporization and for irreversible compaction. This report extends previous work by the same authors by taking into account release adiabat data in selecting empirical coefficients for the equations of state.

DD FORM 1 JAN 64 1473

I-A

UNCLASSIFIED
Security Classification

14. KEY WORDS	LINK A		LINK B		LINK C	
	ROLE	WT	ROLE	WT	ROLE	WT
Equation of State Granite Tonalite Anorthosite Limestone Sandstone Basalt Tuff (wet and dry) Salt						

INSTRUCTIONS

1. **ORIGINATING ACTIVITY:** Enter the name and address of the contractor, subcontractor, grantee, Department of Defense activity or other organization *(corporate author)* issuing the report.

2a. **REPORT SECURITY CLASSIFICATION:** Enter the overall security classification of the report. Indicate whether "Restricted Data" is included. Marking is to be in accordance with appropriate security regulations.

2b. **GROUP:** Automatic downgrading is specified in DoD Directive 5200.10 and Armed Forces Industrial Manual. Enter the group number. Also, when applicable, show that optional markings have been used for Group 3 and Group 4 as authorized.

3. **REPORT TITLE:** Enter the complete report title in all capital letters. Titles in all cases should be unclassified. If a meaningful title cannot be selected without classification, show title classification in all capitals in parenthesis immediately following the title.

4. **DESCRIPTIVE NOTES:** If appropriate, enter the type of report, e.g., interim, progress, summary, annual, or final. Give the inclusive dates when a specific reporting period is covered.

5. **AUTHOR(S):** Enter the name(s) of author(s) as shown on or in the report. Enter last name, first name, middle initial. If military, show rank and branch of service. The name of the principal author is an absolute minimum requirement.

6. **REPORT DATE:** Enter the date of the report as day, month, year, or month, year. If more than one date appears on the report, use date of publication.

7a. **TOTAL NUMBER OF PAGES:** The total page count should follow normal pagination procedures, i.e., enter the number of pages containing information.

7b. **NUMBER OF REFERENCES:** Enter the total number of references cited in the report.

8a. **CONTRACT OR GRANT NUMBER:** If appropriate, enter the applicable number of the contract or grant under which the report was written.

8b, 8c, & 8d. **PROJECT NUMBER:** Enter the appropriate military department identification, such as project number, subproject number, system numbers, task number, etc.

9a. **ORIGINATOR'S REPORT NUMBER(S):** Enter the official report number by which the document will be identified and controlled by the originating activity. This number must be unique to this report.

9b. **OTHER REPORT NUMBER(S):** If the report has been assigned any other report numbers *(either by the originator or by the sponsor)*, also enter this number(s).

10. **AVAILABILITY/LIMITATION NOTICES:** Enter any limitations on further dissemination of the report, other than those imposed by security classification, using standard statements such as:

(1) "Qualified requesters may obtain copies of this report from DDC."

(2) "Foreign announcement and dissemination of this report by DDC is not authorized."

(3) "U. S. Government agencies may obtain copies of this report directly from DDC. Other qualified DDC users shall request through _____."

(4) "U. S. military agencies may obtain copies of this report directly from DDC. Other qualified users shall request through _____."

(5) "All distribution of this report is controlled. Qualified DDC users shall request through _____."

If the report has been furnished to the Office of Technical Services, Department of Commerce, for sale to the public, indicate this fact and enter the price, if known.

11. **SUPPLEMENTARY NOTES:** Use for additional explanatory notes.

12. **SPONSORING MILITARY ACTIVITY:** Enter the name of the departmental project office or laboratory sponsoring *(paying for)* the research and development. Include address.

13. **ABSTRACT:** Enter an abstract giving a brief and factual summary of the document indicative of the report, even though it may also appear elsewhere in the body of the technical report. If additional space is required, a continuation sheet shall be attached.

It is highly desirable that the abstract of classified reports be unclassified. Each paragraph of the abstract shall end with an indication of the military security classification of the information in the paragraph, represented as *(TS), (S), (C), or (U)*

There is no limitation on the length of the abstract. However, the suggested length is from 150 to 225 words.

14. **KEY WORDS:** Key words are technically meaningful terms or short phrases that characterize a report and may be used as index entries for cataloging the report. Key words must be selected so that no security classification is required. Identifiers, such as equipment model designation, trade name, military project code name, geographic location, may be used as key words but will be followed by an indication of technical context. The assignment of links, rules, and weights is optional.

DNA 2925Z
AA-R-7134-2283
September 1972

EQUATIONS OF STATE FOR GEOLOGIC MATERIALS

S. H. Schuster, Applied Theory Inc.
J. Isenberg, Agbabian Associates

THIS WORK SPONSORED BY
THE DEFENSE NUCLEAR AGENCY
UNDER NWER SUBTASK SB 047-08

Prepared for

DEFENSE NUCLEAR AGENCY
Washington, D.C.

AGBABIAN ASSOCIATES
Los Angeles, California

Contract No. DNA001-72-C-0045

CONTENTS

ILLUSTRATIONS

CONTENTS (CONTINUED)

CONTENTS (CONTINUED)

TABLES

SECTION 1

INTRODUCTION

This report considers data and mathematical models for geological materials subjected to shock loading. Data from laboratory experiments are summarized in terms of pressure (P) and density (ρ) at equilibrium states. An ensemble of such states over a range of pressures constitutes the principal Hugoniot for a material. The specific internal energy (e) at these states can be found by applying the Rankine-Hugoniot equations for conservation of mass, momentum, and energy. Data are also given for states along adiabatic pressure release paths. The model must be used cautiously below 50 kb, because variations in density, porosity, and moisture within the same basic material from different locations can dramatically affect the low-pressure properties. The model accounts for these variations if the empirical constants are properly modified. At high levels of pressure and specific internal energy, the model represents a perfect gas (gamma law gas, i.e. $P = (\gamma-1)\rho e$) with $\gamma = 1.5$. Under conditions of very low density and specific internal energy above the vaporization energy (e_m), the model represents a perfect gas with $\gamma = 1.1$.

Analytic equations of state are provided which match approximately the main features of the data over the range mentioned. The equation of state aims primarily to calculate P, once ρ and e are specified. The basic form of the high-pressure model is due to Tillotson (Reference 1-1). However, deviatoric stress/strain relations are accounted for in order to provide a more realistic model in the low-pressure region. The deviatoric stress/strain relations are prescribed by means of a variable-moduli, perfectly plastic model, with associated plastic potential flow rule. This model, when used with a Coulomb-type yield criterion depending on mean stress, produces dilatency or plastic volumetric expansion. This tendency opposes the plastic volumetric compaction, or hysteresis, which enters through the variable bulk modulus. Although rigorous proofs of uniqueness are not generally available for such an analytic model (Reference 1-2), which in any event apply only in the low-pressure range, no difficulties in obtaining unique solutions have been encountered in practice.

The major modifications to previous work done in this area (References 1-3 and 1-4) include accounting for (1) the specific energy lost or gained during phase changes, (2) changes in bulk and shear moduli and in shear strength due to phase changes, and (3) volumetric compaction due to irreversible closure

of cracks or pore spaces. Also, specific parameters of the model for each material are selected after considering both Hugoniot and release isentrope data.

The materials considered in this study include the following:

NTS Granite (granodiorite)

Cedar City Tonalite

Laramie Anorthosite

Banded Mountain Limestone

Coconino Sandstone

Mountain Home Basalt (dense and porous)

Tuff

Salt

The data on which each model is derived are obtained primarily from laboratory experiments on samples whose maximum dimension is 1 to 2 in. Site surveys are also considered for general rock classification, in situ bulk density, porosity, water content, seismic velocity, crack patterns, and geologic layering. It is common in such a survey to find variations of as much as 10 to 15 percent in as basic a property as the density. Other properties, such as porosity or seismic velocity, may easily vary more than a factor of two within a geological area much smaller than the region considered in a ground motion calculation. Judgment is a necessary ingredient, therefore, in selecting representative values for each of the parameters measured in these surveys.

Because the tests included in a site survey are performed at low pressure, one must turn to laboratory results to obtain the high-pressure dynamic properties of the rock. However, the site surveys are useful for identifying the specimens which are most representative of the in situ medium and, based on the homogeneity of the site, for determining how extensive the laboratory programs must be to describe the rock in the field. At mean stress levels less than a few kilobars, the triaxial and hydrostatic tests provide most of the data necessary to determine the values of the parameters in the constitutive model. The hydrostat provides the relation between mean stress and relative volume, and triaxial tests are used to determine the shear modulus and yield criterion. Loading and unloading cycles in both types of tests are necessary to measure the extent of hysteretic compaction in porous media at various loading stresses. Wave speed measurements and low-pressure

Hugoniot data provide a useful check on these properties. At high pressures, the Hugoniot data provide a measure of the material's elastic limit and its behavior up to energy densities at which the Thomas-Fermi theory (i.e., perfect gas with $\gamma = 1.5$) can be applied. Release isentropes from multikilobar shock states help complete the description of hysteretic compaction.

REFERENCES

1-1. Tillotson, J., *Metallic Equations of State for Hypervelocity Impact*, GA 3216, General Atomic Division, General Dynamics Corporation, July 1962.

1-2. Bleich, H. H., *On the Use of A Special Nonassociated Flow Rule for Problems of Elasto-Plastic Wave Propagation*, DASA 2635, Paul Weidlinger Consulting Engineering, March 1971.

1-3. Allen, R. T., *Equations of State of Rocks and Minerals*, GAMD-7834, General Atomic Division of General Dynamics, March 17, 1967.

1-4. Schuster, S. H., and J. Isenberg, *Free Field Ground Motion for Beneficial Facility Siting, Volume 2--Equations of State for Geologic Media*, SAMSO-TR-70-88, Applied Theory, Inc.-Agbabian-Jacobsen Associates, June 30, 1970.

SECTION 2

GENERAL EQUATIONS OF STATE

The general equations of state are divided into two parts. The first part describes calculation of the pressure or mean stress and the second part describes calculation of deviatoric stresses in the solid phase. In the fluid state, the deviatoric stresses vanish and only the first part of the EOS is necessary.

CALCULATION OF PRESSURE OR MEAN STRESS

Loading

The mean stress or pressure is expressed as the sum of two independent parts: the fluid pressure (P_f) and the solid pressure (P_s).

$$P = P_f + P_s \tag{2-1}$$

Since the pressure in a fluid is assumed to be independent of its previous history, P_f is a function of only specific internal energy (e) and density (ρ). The equations for calculating the fluid pressure are a modification of the model first proposed by J. Tillotson (Reference 2-1), for metals subjected to strong shocks:

$$P_f = \left[a_1 + \left(a_2 + \frac{b}{\frac{e}{e_o \eta^2} + 1} \right) \exp Z \rho e^* \right] \tag{2-2}$$

where

a_1, a_2, b, e_o = Empirical constants

$\eta = \frac{\rho}{\rho_o}$ (ρ_o is reference density)

and

		Criterion	Material State
Z	$= \begin{cases} 0 \\ \alpha \frac{\mu}{\eta} \end{cases}$	$\mu \geq 0$ $\mu < 0$	Liquid or compressed gas Expanded gas
e^*	$= \begin{cases} 0 \\ e - e_m \end{cases}$	$e \leq e_m$ $e > e_m$	Cold solid Fluid with specific internal energy greater than that required to begin the phase change (e_m) from the solid state

The specific internal energy at which the phase change is initiated depends on the compression η

$$e_m = e_{mo} (1 + f\eta) \leq e_{mm}$$

where

e_{mo} = Specific internal energy required to initiate a phase change at normal density

e_{mm} = Specific internal energy at which a phase change is completed

f = Empirical parameter

The role of $\exp z$ is to provide a smooth transition from the compressed state to that of an ideal, low density gas. The reason for defining a new variable, e^*, to represent the internal energy is to account for the energy absorbed or released during a phase change which does not affect pressure or density. Thus, on loading, there is no contribution to P from P_f until $e = e_m$. As loading continues and $e > e_m$, it is shown below that the contribution of P_s rapidly decreases and is replaced by P_f. Conversely, as unloading proceeds from a fluid state, the main contribution to P is from P_f until $e = e_m$. If unloading continues such that $e < e_m$, P_s becomes the dominant contributor.

Under conditions of low density and high internal energy, Equation 2-2 effectively reduces to

$$P_f = a_1 \rho e^* \qquad (2\text{-}3)$$

This is the familiar equation for a low density perfect gas in which $a_1 = \gamma - 1$ where γ is the ratio of the specific heats at constant pressure and volume. For purposes of the calculations, it is assumed that a_1 is a constant, even though γ is known to vary (Reference 2-2) with P, ρ, and e. To minimize the error, an average value of a_1 in the range of interest is selected. The values a_2 and b are chosen to match experimental Hugoniot data at pressures of the order of 500 kb, while e_o is selected so that the model approximates the Thomas-Fermi-Dirac description of highly compressed material at high-energy densities.

Calculation of the mean stress in the solid, P_s in Equation 2-1, is based on J. B. Walsh's concept (References 2-3 and 2-4) that the effective values of the elastic parameters differ from the intrinsic values for the consolidated material due to the presence of cracks and pores. The hydrostatic loading behavior of a material containing cracks and pores is then described by a bulk modulus which varies in the following way:

$$\frac{\partial P_s}{\partial \mu} = K_m - (K_m - K_o) \exp\left(\frac{-\mu}{\mu^*}\right) \qquad (2\text{-}4)$$

where

K_o = Initial bulk modulus

K_m = Intrinsic bulk modulus

μ = Elastic component of excess compression = $\frac{\rho}{\rho_o} - 1$

μ^* = Empirical constant

Integrating Equation 2-4 between the limits 0 and $\mu + \beta e$ (β is the coefficient of volumetric thermal expansion per unit energy), leads to the following equation for P_s:

$$P_s = K_m (\mu + \beta e) - (K_m - K_o)\, \mu^* \left[1 - \exp \frac{-\mu - \beta e}{\mu^*}\right] \qquad (2\text{-}5)$$

Initially, $\mu + \beta e = 0$ and the bulk modulus is K_o, the bulk modulus of the rock matrix with included voids. As μ increases the voids close, and the bulk modulus approaches the intrinsic value K_m. The function of the empirical constant μ^* is to control the rate at which the solid bulk modulus asymptotically

approaches its maximum value. In selecting a value of μ^* for a specific material, it is helpful to remember that $\partial P_s/\partial \mu$ will approach K_m faster as μ^* is made smaller. This formulation assumes that the mean stress depends only on the elastic component of volume change. Inelastic volume change due to plasticity and strain rate effects are specifically excluded from computation of pressure.

P_s depends on e in two ways. First, μ is augmented by the thermal expansion, βe, so that a hot solid is at a higher pressure than a cold one at the same density. Also, since the intrinsic bulk modulus of most rocks decreases with increasing temperature or energy (Reference 2-5), K_m in Equation 2-5 is replaced by

$$K_m = K_{max}\left[1 - \left(c\,\frac{e}{e_m}\right)\right] = K_{max}\left[1 - \frac{ce}{e_{mo}(1 + fn)}\right] \geq 0 \qquad (2\text{-}6)$$

where

K_{max} = Intrinsic bulk modulus at room temperature

c = Empirical constant

Thus, the solid contribution to the effective bulk modulus becomes zero when the phase change is initiated. The effect of causing the bulk modulus to decrease with increasing specific internal energy is to make a portion of the principal Hugoniot to be concave to the y-axis, as is illustrated in Figure 2-1. In selecting values of the parameters c and f for a specific material, it is helpful to remember that point m moves toward the origin if c is increased, if e_{mo} is decreased, or both.

The model described above is adequate for materials whose initial porosity is less than about 5 percent. For materials with greater initial porosity, the very low-pressure, solid-phase hydrostat is modified as shown in Figure 2-2(a). The material is assigned a reference density ρ_{ref}, which is assumed to be the density at zero pressure along a master unloading curve as shown in Figure 2-2. A new variable $\bar{\mu}$ is defined, which enables the P/μ relation on loading to be calculated from the master unloading relation. Thus

$$P = P(\bar{\mu})$$

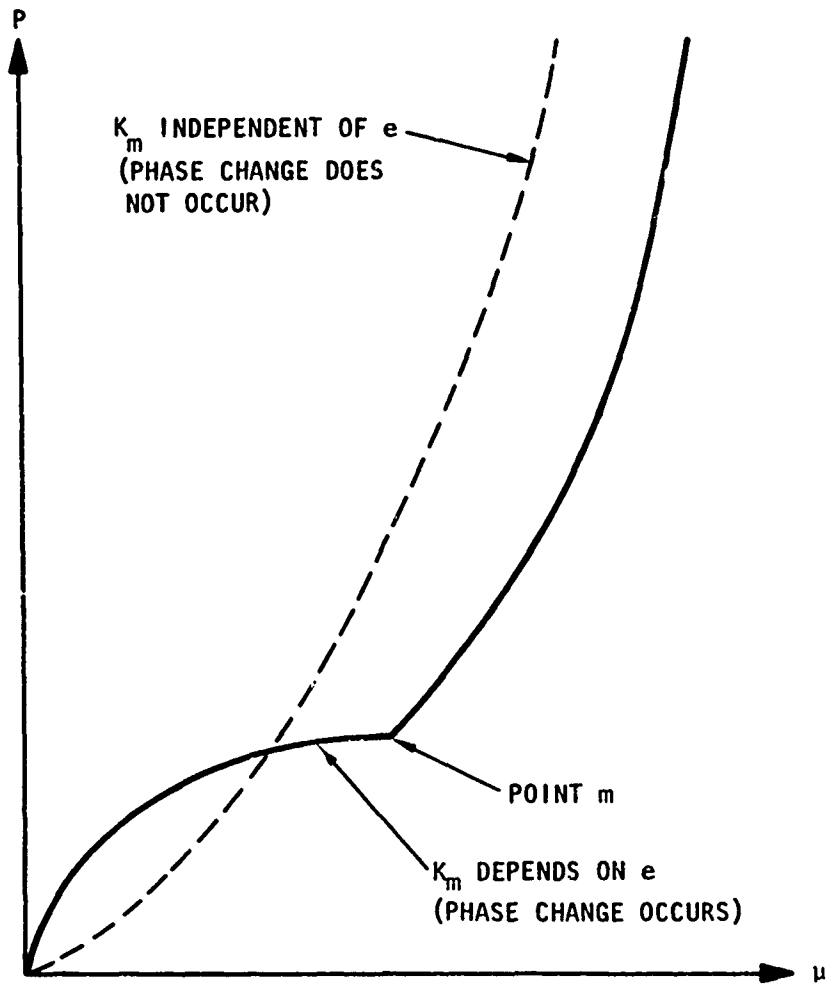

FIGURE 2-1. HYDROSTAT FOR TWO MATERIALS, ONE OF WHICH EXHIBITS A PHASE CHANGE IN THE PRESSURE RANGE INDICATED

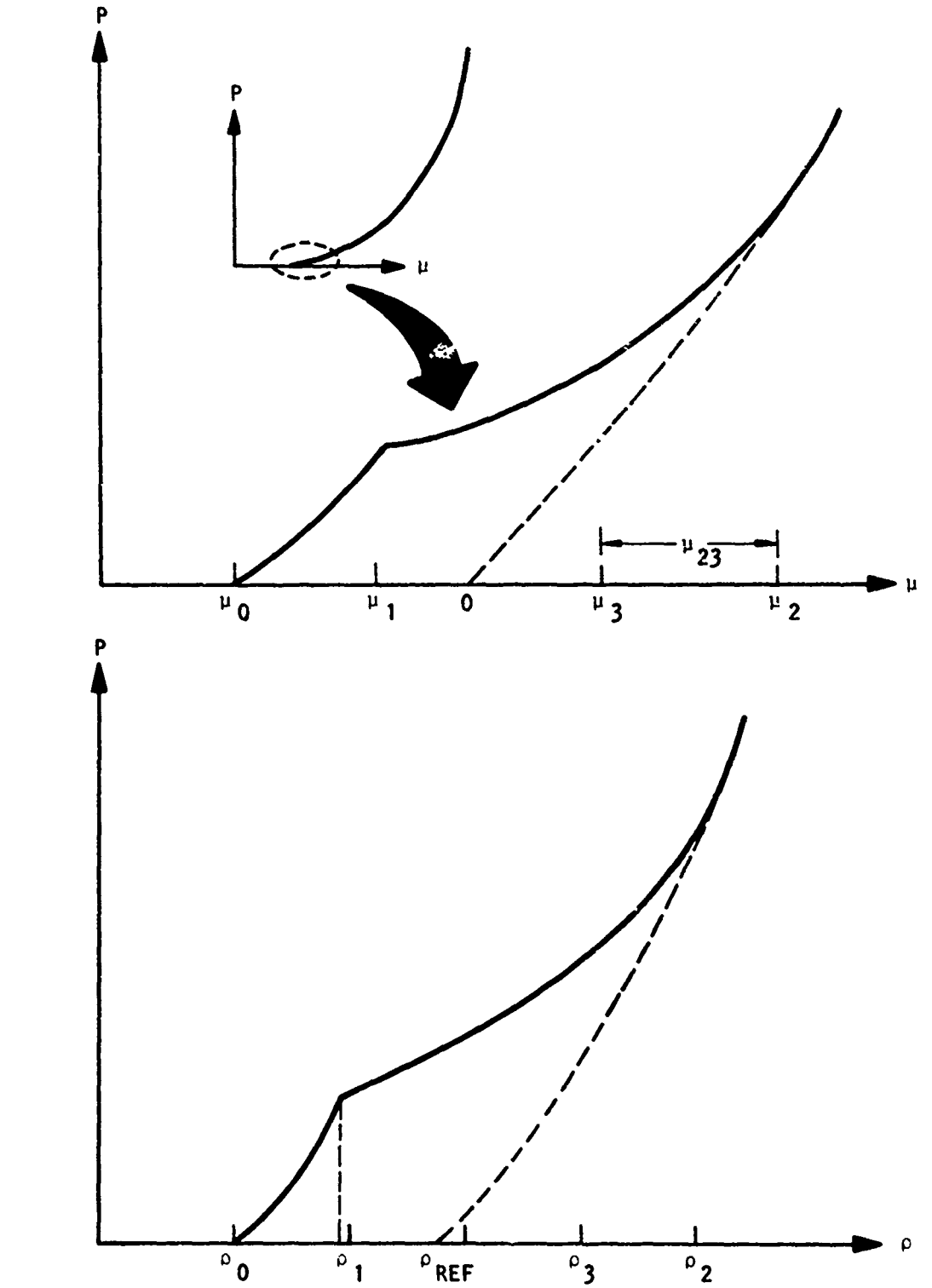

FIGURE 2-2. LOW PRESSURE HYDROSTAT FOR A HIGHLY POROUS MATERIAL

where

Region	μ	$\bar{\mu}$
1	$\mu \leq \mu_1$	$\bar{\mu} = \mu - \mu_o$
2	$\mu_1 < \mu < \mu_2$	$\bar{\mu} = \mu_3 + \mu_{23} \exp - \frac{(\mu_2 - \mu_3)}{\mu_{23}}$
3	$\mu_2 \leq \mu$	$\bar{\mu} = \mu$

The empirical parameters μ_1, μ_2, and μ_3 have the following physical interpretation:

μ_1 = Excess compression, at which the material matrix begins to break down

μ_2 = Excess compression, at which the virgin loading curve joins the master unloading curve

$\mu_3 = \mu_1 - \mu_o$

Unloading

In the present model, primary consideration during unloading is given to hysteresis, the irreversible compaction which may occur during a cycle of hydrostatic loading and unloading. As an example, experimental data (Reference 2-6) indicate that NTS granite compacts irreversibly to about 1.005 times its initial density when it is subjected to pressures between 5 and 50 kb and then unloaded. If the peak loading pressure is less than 5 kb, the hysteretic compaction is less than 0.005, but because the unloading data are limited, the functional relationship between the permanent compaction and peak pressure in this regime is based on hypothesis.

The mathematical procedure for representing hysteresis is an extension of the variable modulus method used for the loading relationship. If μ is greater than or equal to the maximum excess compression (μ_m) previously experienced by the material, P_s is calculated by Equation 2-5, which is referred to as the virgin loading curve. However, if $\mu < \mu_m$, the material is on an unloading/reloading path. The permanent compaction or "set" resulting from loading to μ_m is then calculated. This set represents a new point along the μ-axis, namely μ_z, at which

the mean stress returns to zero. The unloading path has the same value of pressure, P_m, as the virgin loading curve when $\mu = \mu_m$. Thus, if K_m and μ^* are assumed to be constant. Equation 2-6 can be inverted to obtain a new value of K_o, namely

$$K_o' = K_m - \left| P_m - K_m(\mu_m - \mu_z + \beta e) \right| x$$

$$\left| \mu^* \left\{ 1 - \exp \left[- \left(\mu_m - \mu_z + \beta e \right) \mu^* \right] \right\} \right| \qquad (2\text{-}7)$$

Along an unloading path P_s then becomes

$$P_s = K_m(\mu' + \rho e) - \left(K_m - K_o' \right) \mu^* \left(1 - \exp\left[\frac{-\mu' - \beta e}{\mu^*} \right] \right) \qquad (2\text{-}8)$$

where

$$\mu' = \mu - \mu_z$$

If the solution of Equation 2-7 produces a value of K_o' larger than K_m, which is presumably the maximum bulk modulus, it is assumed that a phase change has occurred and the material is constrained to unload along the linear path:

$$P = K (\mu' + \beta e) \qquad (2\text{-}9)$$

where K is $P_m/(\mu_m - \mu_z)$.

The definition of μ_z completes the specification of P_s. Experimental data (References 2-6, 2-7, and 2-8) show that μ_z increases with increasing peak pressure until all of the cracks and voids are apparently closed. Further moderate increase in pressure does not appreciably increase the permanent set. At very high pressures, μ_z may again increase due to phase changes in one or more of the constituent minerals in the rock. This behavior, depicted schematically in Figure 2-3, is expressed mathematically by

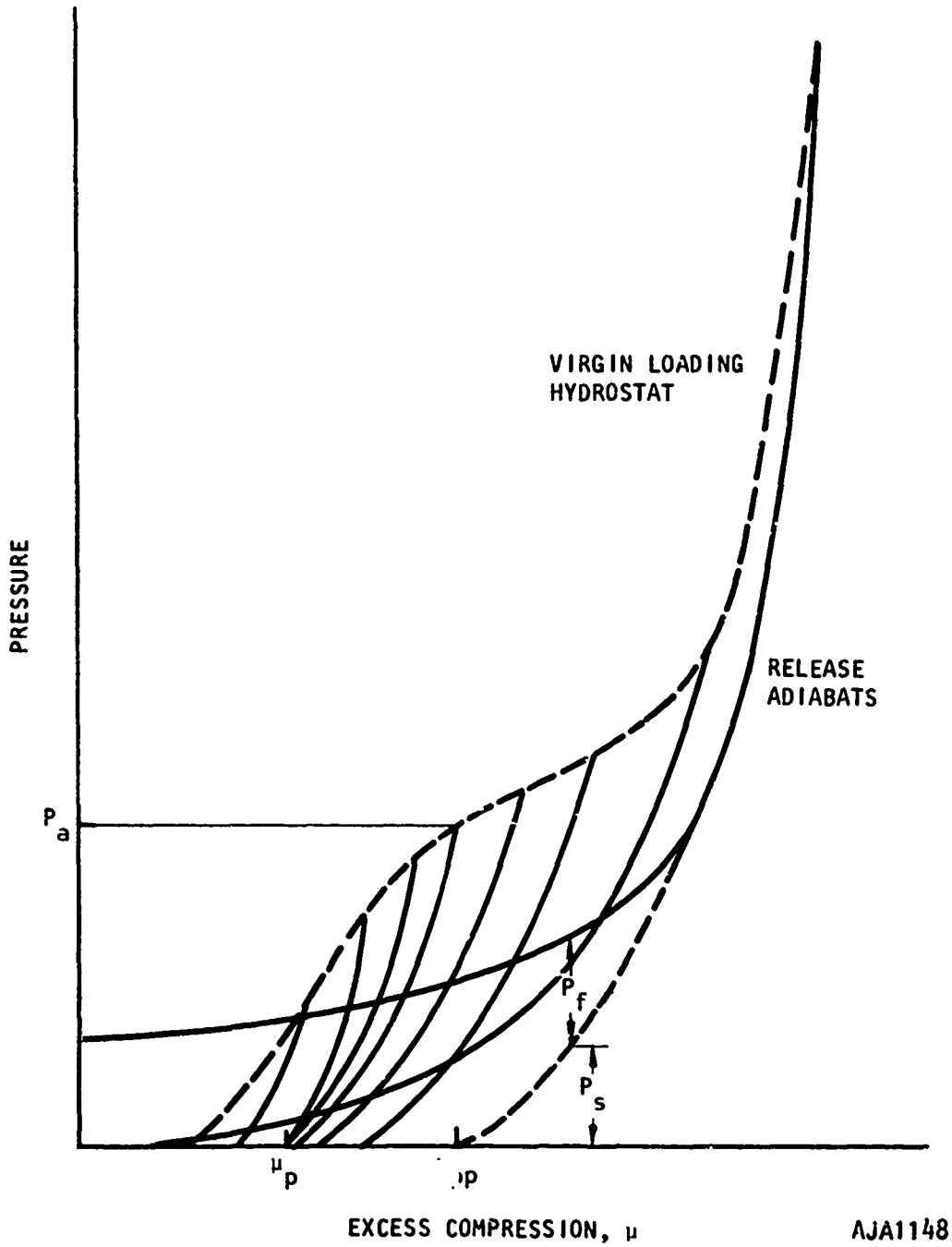

FIGURE 2-3. IDEALIZED HYDROSTAT AND RELEASE ADIABATS ILLUSTRATING THE EFFECT OF HYSTERETIC COMPACTION ON P_s

Criterion

$$\mu_z = \begin{cases} P_m d & P_m \leq \mu_p/d \\ \mu_p & \mu_p/d \leq P_m \leq P_a \\ \mu_p + (P_m - P_a)\, d & P_a < P_m \cdot \dfrac{\mu_{pp} - \mu_p}{d} + P_a \\ \mu_{pp} & \dfrac{\mu_{pp} - \mu_p}{d} + P_a \leq P_m \end{cases} \qquad (2\text{-}10)$$

μ_p is the excess compression at which all the voids are closed. The density ρ_p ($= \rho_o(1 + \mu_p)$) must be less than or equal to the crystal density of the rock. P_a is the minimum pressure at which a phase change can occur and ($= \rho_o(1 + \mu_{pp})$) is the crystal density of the rock after the phase change is completed. The assumption that μ_z varies linearly with pressure (d is the proportionality constant) is certainly crude, but the meager unloading data and the large scatter within that data does not justify further refinements at this time.

For the highly porous type of material whose loading hydrostat is illustrated in Figure 2-2, the pressure during unloading is found by evaluating Equations 2-7 and 2-8 with $\mu' = \mu - \mu_o$. The result of this procedure is an unloading hydrostat which passes through the point (P_m, μ_m) and is parallel to the master curve. Hysteresis is automatically accounted for during the loading phase.

In using this model in practical calculations, mean tensile stresses may develop. Because of the low value of tensile strength for in situ rock, this is prevented and P_s is set equal to zero for $\mu < \mu_z$.

CALCULATION OF DEVIATORIC STRESS

A complete description of the material in the solid state requires the specification of deviatoric stresses (σ'_{ij}) as well as the mean stress. If the material behaves elastically, the stress increment is calculated from

$$d\sigma'_{ij} = 2G(d\varepsilon'_{ij}) \qquad (2\text{-}11)$$

where

$d\epsilon'_{ij}$ = Deviatoric strain increment

G = Shear modulus

Stress states are calculated incrementally to allow for the possibility of plastic deformations. A trial deviatoric stress tensor is calculated at the end of each time step from

$$(\sigma'_{ij})_{trial} = (\sigma'_{ij})_{old} + (d\sigma'_{ij}) \qquad (2\text{-}12)$$

where $d\sigma'_{ij}$ is obtained from Equation 2-11. A yield criterion is used to determine whether the deviatoric stress $(\sigma'_{ij})_{trial}$ defines an elastic state. If so, then $(\sigma'_{ij})_{trial}$ is the correct deviatoric stress, otherwise, plastic deformation has occurred during the time step, and $d\sigma'_{ij}$ must be adjusted according to the yield criterion and the associated plastic potential flow rule.

The mathematical model of the shear modulus G is similar to that of the bulk modulus. G varies from an initial value, G_o, at normal density, to the intrinsic value, G_{max}, as the pores and cracks are closed.

$$G = G_{max} - (G_{max} - G_o) \exp \frac{-\mu}{\mu^*_G} \qquad (2\text{-}13)$$

Some experimental data (References 2-9 and 2-10) indicate that, for rock which has been cracked prior to testing, G_o is close to zero. (Reference 2-6 reports $G_o = 0 \pm 4$ kb for fractured NTS granite.) However, as μ increases, G approaches its intrinsic value much more rapidly than does K. We assume that variability of the effective bulk modulus is strongly affected by the closing of spherical pores, whereas the effective shear modulus is more influenced by the closing of in situ cracks. It is consistent with the findings of Reference 2-3, which shows that cracks are more easily closed than pores, for G to approach its intrinsic value faster than does K.

Specifying that G increases with increasing μ raises the possibility that energy might be extracted from the material by hydrostatically compressing it, shearing it at high pressure, releasing the pressure, and then releasing the shear. This danger is avoided by assuming that friction prevents cracks from reopening during unloading so that the largest value of G reached on loading is retained during subsequent unloading/reloading. Under these restrictions, a material may dissipate energy in shear during loading and unloading cycles but can never produce additional energy.

Data on the temperature dependence of material strength (Reference 2-11) clearly indicate that the shear strength of several rocks decreases almost linearly with increasing temperature. By analogy, a similar dependence is assumed for the shear modulus. As the specific internal energy approaches e_m, G tends towards zero according to the following equation:

$$G = \left[G_{max} - (G_{max} - G_o) \exp \frac{-\mu}{G}\right]\left(1 - \frac{e}{e_m}\right) \qquad (2\text{-}14)$$

For $e > e_m$, the rock is assumed to have undergone a phase change such as melting, and to be unable to support shear stress, in which case the shear modulus, G, is set to zero.

The yield criterion determines the maximum deviatoric stress which the material can support before it deforms plastically. The yield criterion is a function of stress components. If the criterion is not satisfied, the material is assumed to behave elastically. If the trial deviator stresses calculated by Equation 2-11 are in the forbidden region outside the yield surface, the stress state is adjusted by means of the flow rule so as to be exactly on the yield surface. The yield surface used is a combination of the Mohr-Coulomb and von Mises representations (Reference 2-12), i.e.,

$$\sqrt{J_2'} = Y = \text{minimum of} \begin{cases} k_1 + k_2 P \\ k_3 \end{cases} \qquad (2\text{-}15)$$

where

J_2' = Second invariant of the stress deviator; a function of the current state of stress

k_1 = Cohesion

k_2 = Tangent of the angle of internal friction

k_3 = Upper limit of yield strength (von Mises Surface)

Towles and Riecker (Reference 2-11) have shown that the shear strength of several rocks decreases with increasing temperature roughly in accord with the following empirical relation:

$$Y = Y_o \exp (tT/T_m) \qquad (2\text{-}16)$$

where t is a negative empirical constant whose value for the rocks tested lies between -0.87 and -1.4, and

T = Temperature

T_m = Melting temperature

Y_o = Shear strength at room temperature

To include temperature effects in the model, the exponential factor in Equation 2-16 is represented by the first two terms of its Taylor series expansion, t is assumed to equal -1, and T/T_m is replaced by e/e_m, assuming constant heat capacity. Thus, Equation 2-15 becomes

$$\sqrt{J_2'} = Y = \text{minumum of} \begin{cases} k_1 + k_2 P \\ k_3\left(1 - \dfrac{e}{e_m}\right) \end{cases} \qquad (2\text{-}17)$$

As the specific internal energy e approaches the melting energy e_m and the solid approaches the fluid state, the stress deviators are reduced to zero by both the shrinking of the von Mises portion of the yield surface and the reduction of the shear modulus G.

The plastic potential flow rule, used to calculate deviatoric stress increments from strain increments when the material is deforming plastically, can be summarized by the statement that among all stress states which lie on the yield surface, the stress actually reached in a given plastic strain increment is one for which the plastic work increment is stationary. The mathematical formulation of this flow rule is discussed more fully in Reference 2-13. This flow rule requires the separation of the strain tensor into elastic and plastic components and can result in permanent plastic volume change. To calculate P_s after plastic volume change has occurred, the elastic component of excess compression μ is used instead of the total excess compression, where

$$\frac{1}{\mu^e + 1} = \frac{1}{\mu + 1} - \frac{1}{\mu^P + 1} \qquad (2\text{-}18)$$

and μ^P is the component of excess compression arising from the plastic flow.

REFERENCES

2-1. Tillotson, J., *Metallic Equations of State for Hypervelocity Impact*, GA 3216, General Atomic Div., General Dynamics Corporation, July 1962.

2-2. Butkovitch, T. R., *The Gas Equation of State for Natural Materials*, UCRL-14729, Lawrence Radiation Laboratory, January 1967.

2-3. Walsh, J. B., "The Effect of Cracks on the Compressibility of Rock," *J. Geophys. Res.*, Vol. 70, No. 2, January 15, 1965.

2-4. Walsh, J. B., "The Effect of Cracks on Poisson's Ratio," *J. Geophys. Res.*, Vol. 70, No. 20, October 15, 1965.

2-5. Anderson, O. L., et al., "Some Elastic Constant Data on Minerals Relevant to Geophysics," *Reviews of Geophysics*, Vol. 6, No. 4, November 1968, p. 491.

2-6. Stephens, D. R., and E. M. Lilley, *Static PV Curves of Cracked and Consolidated Earth Materials to 40 Kilobars*, UCRL-14711, Lawrence Radiation Laboratory, March 1966.

2-7. LaMori, P. N., *Compressibility of Three Rocks, (A) Westerly Granite and Solenhofen Limestone to 40 Kilobars at 300°C, (B) Cedar City Tonalite to 40 Kilobars at Room Temperature*, DASA-2151, Defense Atomic Support Agency, August 1968.

2-8. U. S. Army Corps of Engineers, Missouri River Division Laboratory, *Tests for Strength Characteristics of Rock, Pile Driver Project*, MRDL 64/90, 1964.

2-9. Stephens, D. R., *Elastic Constants of Fractured Granodiorite*, UCID-15369, Lawrence Radiation Laboratory (to be published).

2-10. Calhoun, D. E., *Project Mine Shaft Material Properties*, Preliminary Report, Eric H. Wang Civil Engineering Research Facility, December 1968.

2-11. Towle, L. C., and R. E. Riecker, "The Pressure and Temperature Dependence of the Shear Strength of Minerals," *J. Appl. Phys.*, Vol. 39, No. 10, September 1968, p. 4807.

2-12. Fung, Y. C., *Foundations of Solid Mechanics*, Prentiss-Hall, 1965.

2-13. Trulio, J. G., et al., *Numerical Ground Motion Studies, Vol. III: Ground Motion Studies and AFTON Code Development*, AFWL-TR-67-27, Air Force Weapons Lab, October 1968.

SECTION 3

HUGONIOT AND RELEASE ADIABAT DATA

This section summarizes Hugoniot and release adiabat data for a number of geologic materials whose equation of state has been formulated as described above. The materials considered and the coefficients in the equations are given in Table 3-1.

Comparisons between the equations of state and the relevant data are given in Figures 3-1 through 3-21. For some materials, comparison is made only between data and model along the principal Hugoniot, while for others, data and models for release adiabats are also included. For these materials where release adiabat data are lacking, the model release adiabat is shown centered at 200 kb, 400 kb, 600 kb, and 800 kb.

REFERENCES

3-1. Jones, A. H., and H. H. Froula, *Uniaxial Strain Behavior of Four Geological Materials to 50 Kilobars*, DASA-2209, March 1969.

3-2. Shipman, F. H., et al., *High Pressure Hugoniot Measurements for Several Nevada Test Site Rocks*, DASA-2214, March 1969.

3-3. Grine, D. R., *Equations of State of Granite and Salt*, UCRL-13004, Lawrence Radiation Laboratory, May 1961.

3-4. McQueen, H. G., et al., "Hugoniot Equation of State of Twelve Rocks," *J. Geophys. Res.*, Vol. 72, No. 20, p. 4999, 1967.

3-5. Bass, R. C., *Additional Hugoniot Data for Geological Materials*, SC-RR-66-548, Sandia Corporation, October 1966.

3-6. Bass, R. C., et al., *Hugoniot Data for Some Geological Materials*, SC-4903(RR), Sandia Corporation, June 1963.

3-7. Lombard, D. B., *The Hugoniot Equation of State of Rocks*, UCRL-6311, Lawrence Radiation Laboratory, February 1961.

3-8. Petersen, C. F., *Shock Wave Studies of Selected Rocks*, Ph.D. Thesis, Stanford University, May 1969.

3-9. Keough, D. D., et al., *Piezoresistive Stress--Time Transducer Development and Granite Adiabat Measurements for Project Pile Driver*, DASA-2131, Stanford Research Institute, February 1967.

3-10. Ahrens, T. J., et al., *Dynamic Properties of Rocks*, DASA-1868, Defense Atomic Support Agency, September 1966.

3-11. Saucier, K. L., and D. L. Ainsworth, *Tests of Rock Cores, Warren Siting Area, Wyoming*, MP C-69-3, U. S. Army Engineer Waterways Experiment Station, March 1969.

3-12. Ahrens, T. J., and V. G. Gregson, "Shock Compression of Crystal Rocks: Data for Quart., Calcite, and Plagioclase Rocks," *J. Geophys. Res.*, Vol. 69, No. 22, p. 4839, November 15, 1964.

3-13. Ahrens, T. J., et al., *Dynamic Properties of Rocks*, DASA-1868, Stanford Research Institute, September 1966.

3-14. Isbell, W. M., et al., *The High-Pressure Equation of State for Two Geologic Materials*, General Motors Defense Research Laboratory.

3-15. Lombard, D. B., *The Hugoniot Equation of State of Rocks*, UCRL-6311, Lawrence Radiation Laboratory, February 1961.

3-16. Wiedermann, A. H., et al., *Shock Unloading Characteristics of Porous Geological Materials*, AFWL-TR-66-118, IIT Research Institute, January 1967.

3-17. Altshuler, L. V., *Soviet Physics*, JETP12,10 (1961).

3-18. Rosenberg, J. T., et al., *Dynamic Properties of Rocks*, DASA-2112, Stanford Research Institute, July 1968.

3-19. Lysne, P. C. A., "A Comparison of Calculated and Measured Low-Stress Hugoniots and Release Adiabats of Dry and Water Saturated Tuff," JGR Vol. 75, No. 23, August 1971, p. 4375.

TABLE 3-1. EMPIRICAL COEFFICIENTS FOR EQUATION OF STATE MODELS

	Units	NTS Granite	Cedar City Tonalite	Laramie Anorthosite	Banded Mtn. Limestone	Coconino Sandstone	Porous Basalt	Dense Basalt	Wet Tuff	Dry Tuff	Salt
a_1	-	0.1	0.1	0.1	0.1	0.1	0.1	0.1	0.1	0.1	0.1
a_2	-	0.4	0.4	0.4	0.4	0.4	0.4	0.4	0.4	0.4	0.4
b	-	1.3	1.3	1.3	1.3	0.8	1.0	1.0	1.0	1.1	1.1
c	-	0.35	0.2	0.35	0.2	.	0.35	0.2	0.0	0.0	0.0
d	$mbar^{-1}$	1.0	1.0	0.0	0.855	5.0	1.0	0.0	3.5	3.5	1.0
e_{mo}	$\frac{mbar\text{-}cc}{gm}$	0.0115	0.010	0.0115	0.0007	0.014	0.012	0.0075	0.05	0.05	0.005
e_{mm}	$\frac{mbar\text{-}cc}{gm}$	0.035	0.035	0.035	0.025	0.035	0.035	0.035	0.05	0.05	0.020
e_o	$\frac{mbar\text{-}cc}{gm}$	0.16	0.16	0.16	0.10	0.03	0.16	0.16	0.06	0.06	0.05
f	-	1.7	1.0	1.7	1.7	0.8	0.0	0.0	1.7	1.7	1.0
G_{max}	mbar	0.3	0.1	0.375	0.2	0.045	0.2	0.2	0.04	0.04	0.1
G_o	mbar	0.0	0.1	0.375	0.2	0.045	0.2	0.2	0.04	0.04	0.1
K_{max}	mbar	0.8	0.525	0.8	0.6	0.8	0.5	0.65	0.55	0.55	0.45
K_o	mbar	0.225	0.075	0.6	0.25	0.04	0.15	0.65	0.075	0.075	0.25
k_1	mbar	0.0001	0.0001	0.0001	0.0001	0.00005	0.0001	0.0001	0.0001	0.0001	0.00002
k_2	mbar	0.3	0.3	0.5	0.45	0.75	0.5	0.5	0.78	0.78	0.5
k_3	mbar	0.017	0.00525	0.017	0.003	0.003	0.017	0.017	0.0155	0.0155	0.0005
P_a	mbar	0.05	0.05	0.05	-	0.15	1.0	1.0	0.0	0.0	0.013
t	-	1.0	1.0	1.0	1.0	1.0	1.0	1.0			1.0
α	-	5.0	5.0	5.0	5.0	5.0	5.0	5.0	5.0	5.0	5.0

AA4644

TABLE 3-1. (CONTINUED)

	Units	NTS Granite	Cedar City Tonalite	Laramie Anorthosite	Banded Mtn. Limestone	Coconino Sandstone	Porous Basalt	Dense Basalt	Wet Tuff	Dry Tuff	Salt
β	$\frac{gm}{mbar\text{-}cc}$	3.0	3.0	3.0	3.0	3.0	2.0	2.0	3.0	3.0	15.0
μ_p	-	0.005	0.05	0.0	0.011	0.25	0.16	0.0	0.0	0.0	0.013
μ_{pp}	-	0.4	0.4	0.4	0.011	0.9	0.16	0.16	0.2	0.2	0.013
μ_1	-										
μ_2	-								0.0575	0.0575	
μ_3	-								0.00275	0.00275	
u^*	-	0.3	0.0275	0.03	0.04	1.5	0.05	-	0.1	0.25	0.1
μ^*_G	-	0.005	-	-	-	-	-	-	0.0	-	0.0
ρ_o	gm/cc	2.65	2.55	2.72	2.66	2.0	2.5	2.9	1.76	1.76	2.24
ρ_{ref}	gm/cc	2.65	2.55	2.72	2.66	2.0	2.5	2.9	2.36	2.36	2.24

AA4645

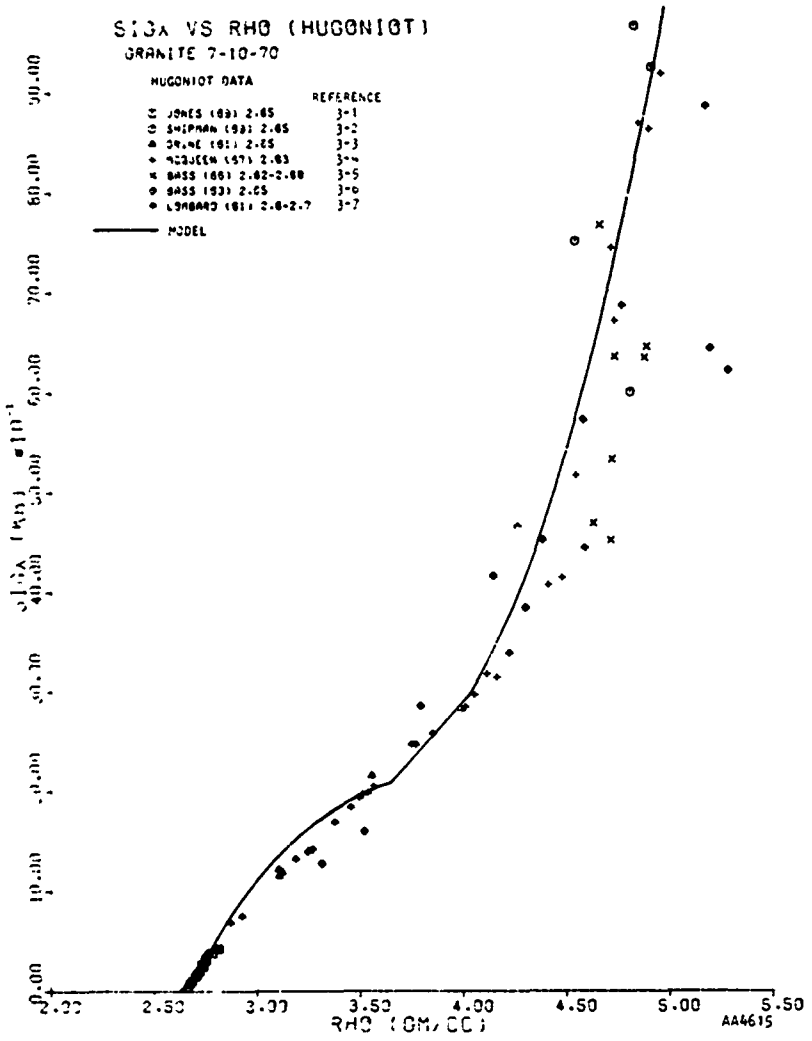

FIGURE 3-1. HUGONIOT DATA AND MODEL FOR NTS GRANITE

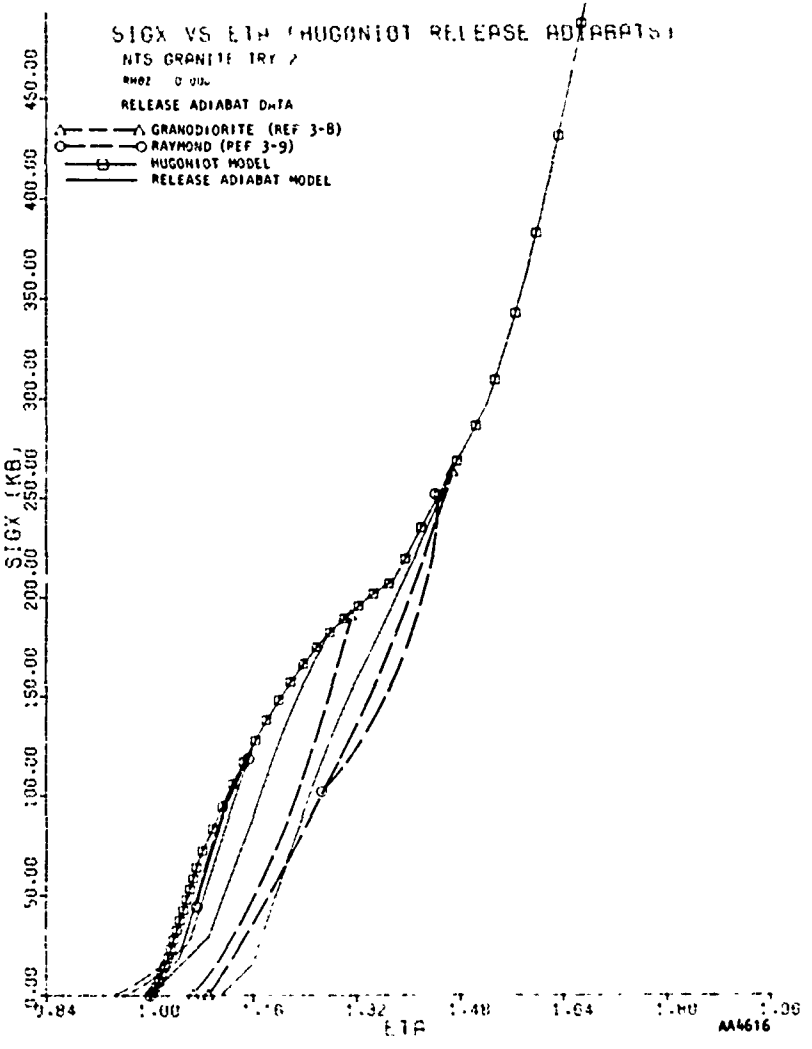

FIGURE 3-2. RELEASE ADIABAT DATA AND MODEL FOR NTS GRANITE

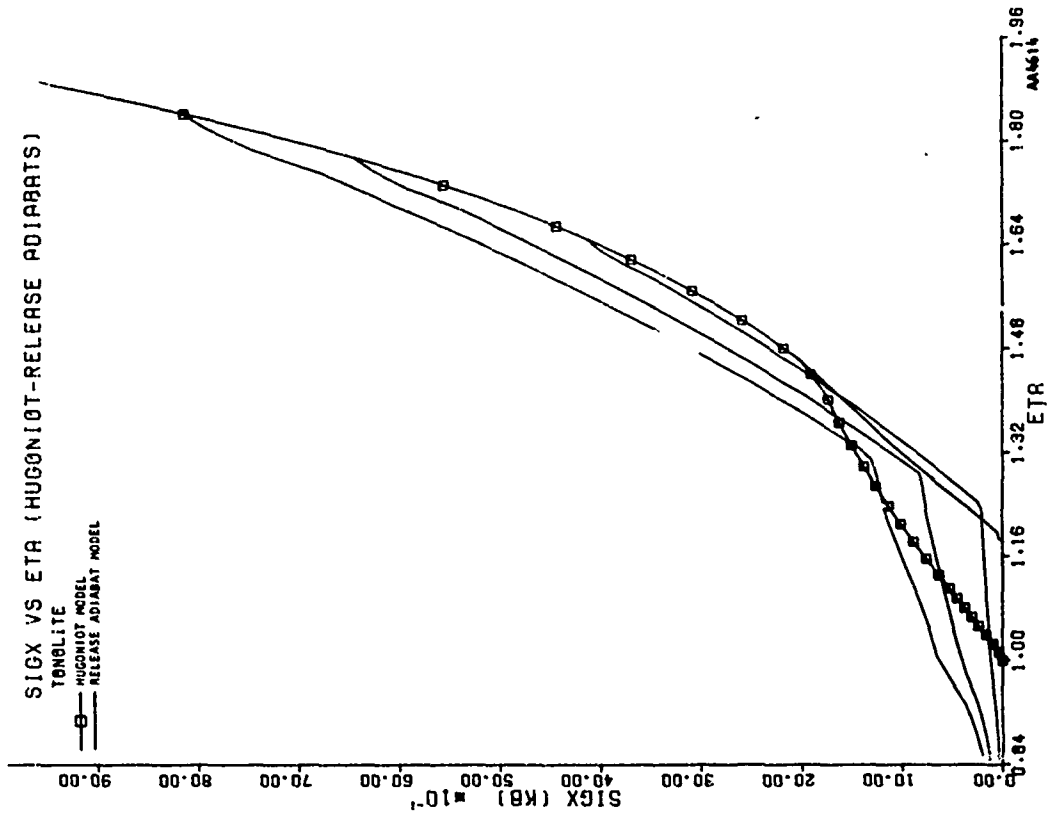

FIGURE 3-4. RELEASE ADIABAT MODEL FOR CEDAR CITY TONALITE

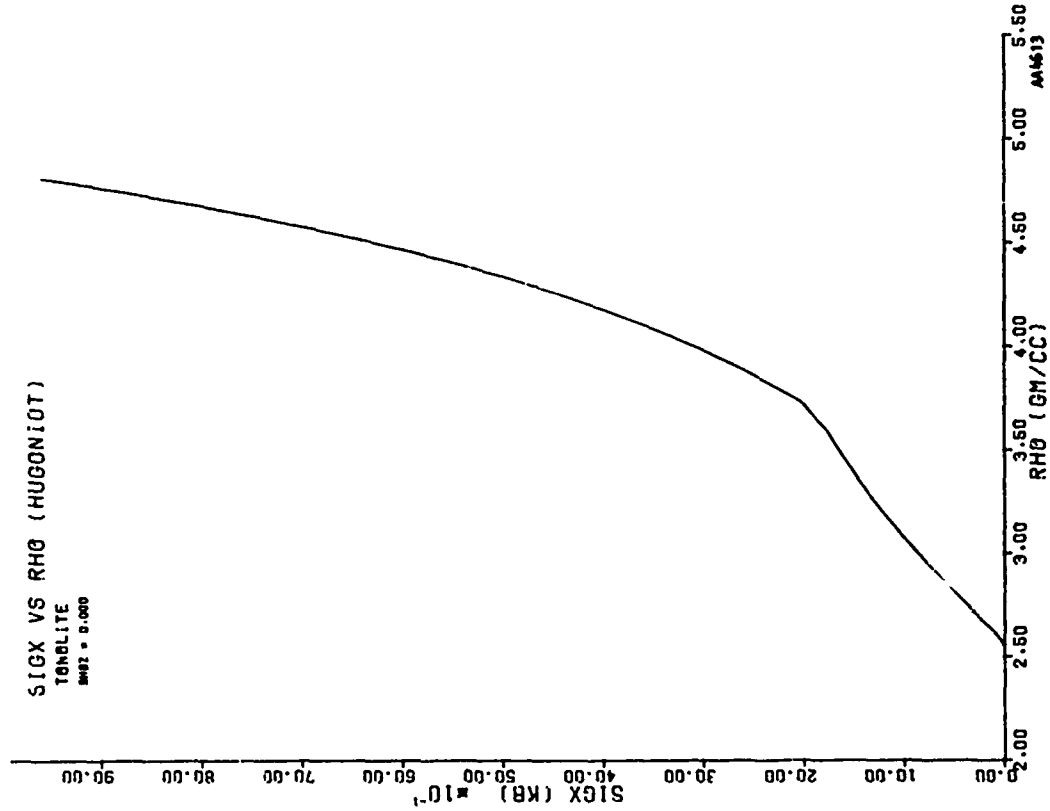

FIGURE 3-3. HUGONIOT MODEL FOR CEDAR CITY TONALITE

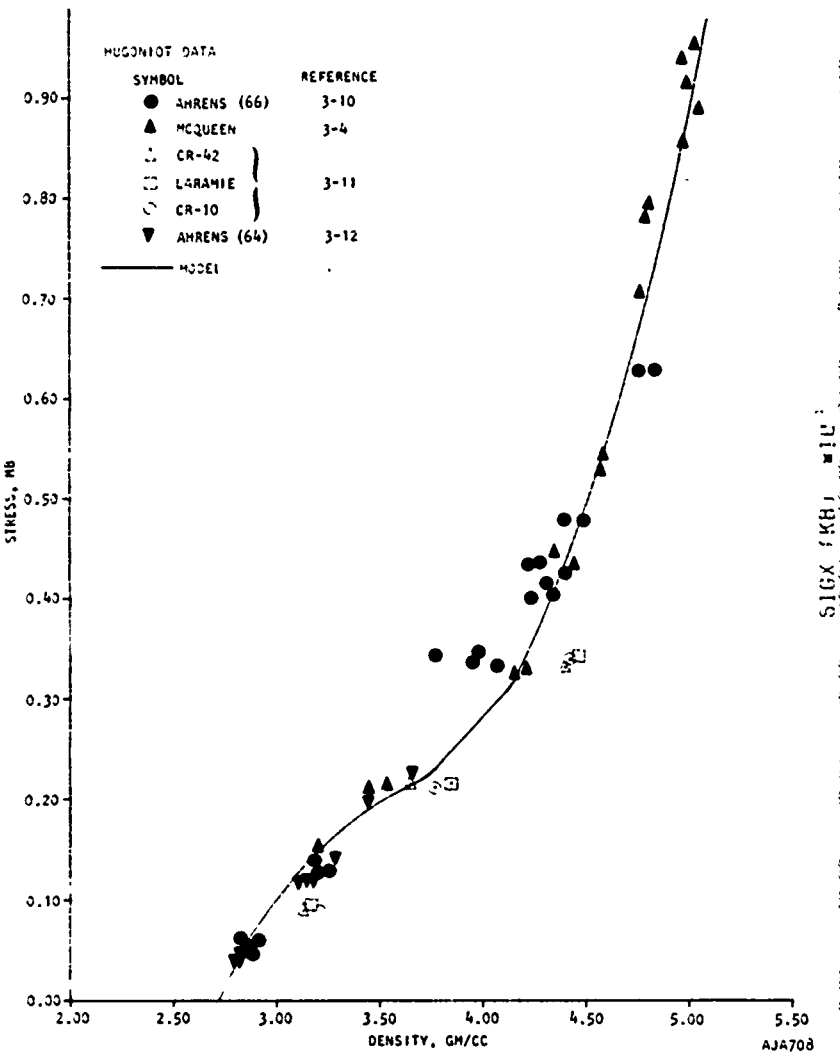

FIGURE 3-5. HUGONIOT DATA AND MODEL FOR LARAMIE ANORTHOSITE

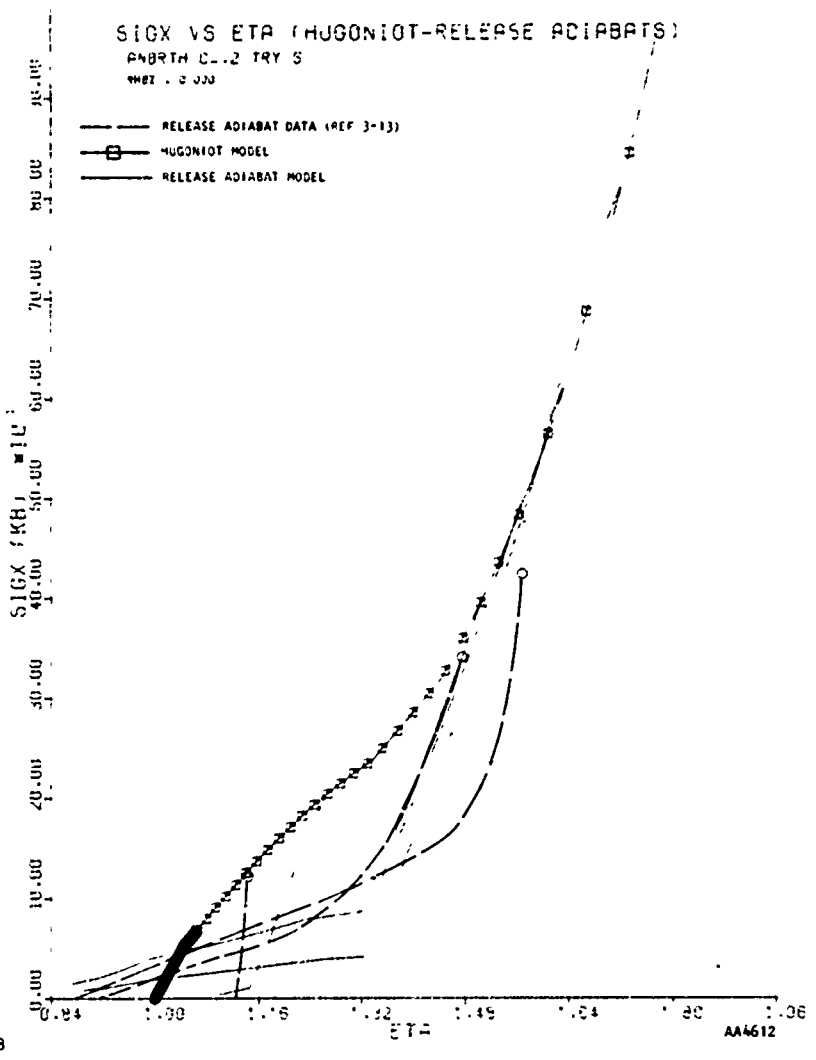

FIGURE 3-6. RELEASE ADIABAT DATA AND MODEL FOR LARAMIE ANORTHOSITE

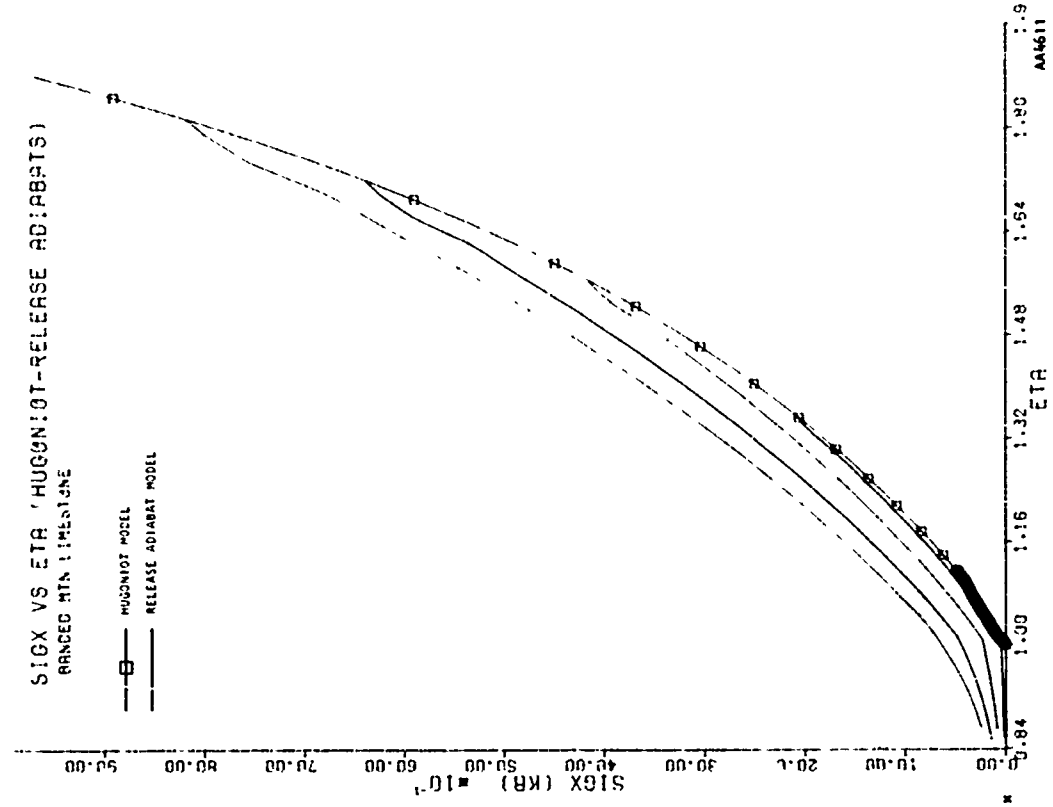

FIGURE 3-6. RELEASE ADIABAT MODEL FOR LIMESTONE

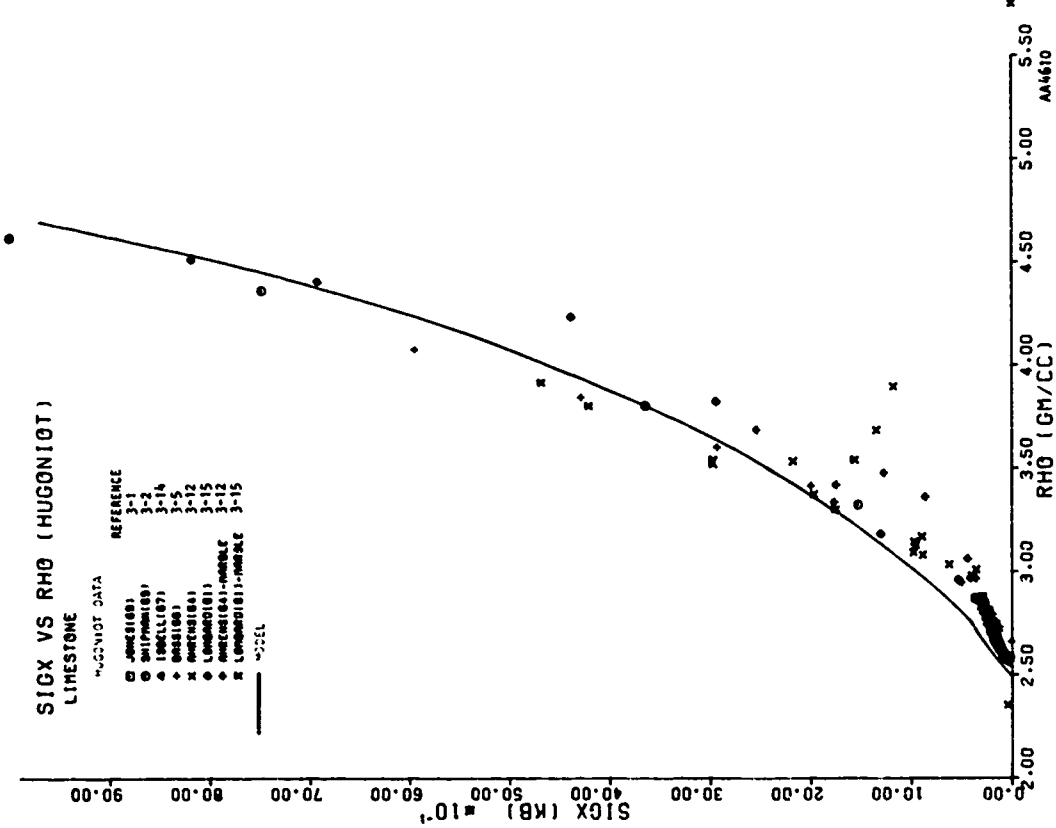

FIGURE 3-7. HUGONIOT DATA AND MODEL FOR LIMESTONE

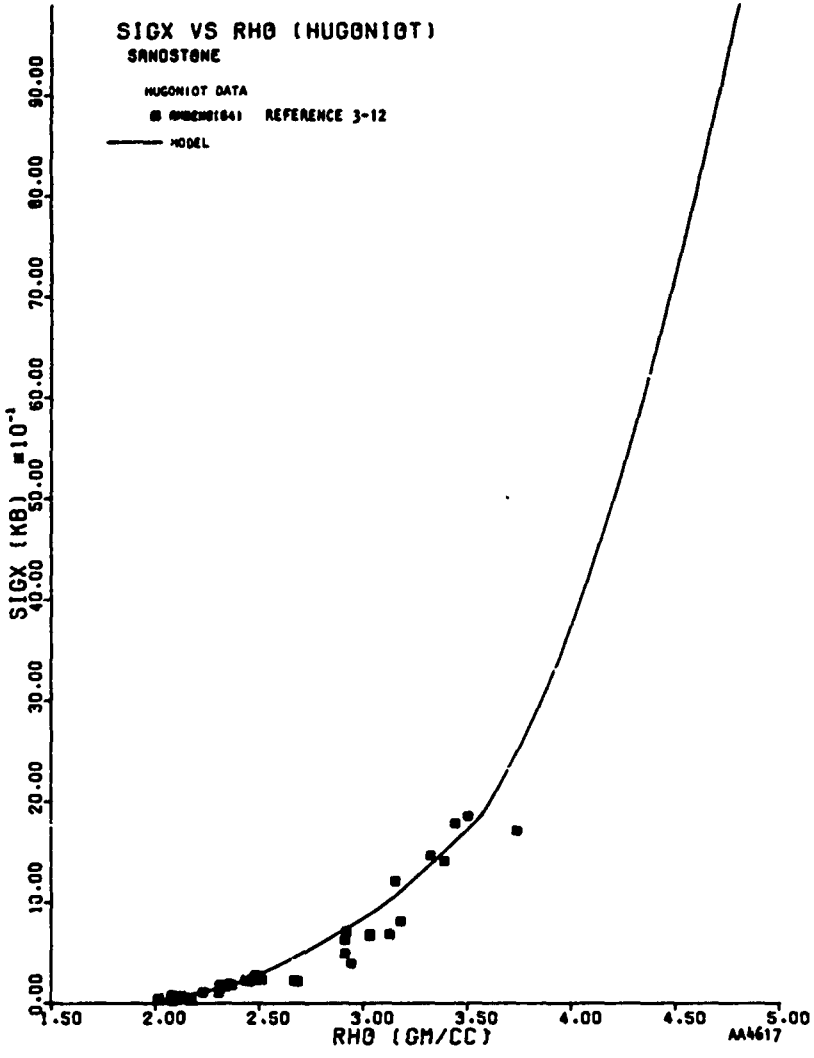

FIGURE 3-9. HUGONIOT DATA AND MODEL FOR SANDSTONE

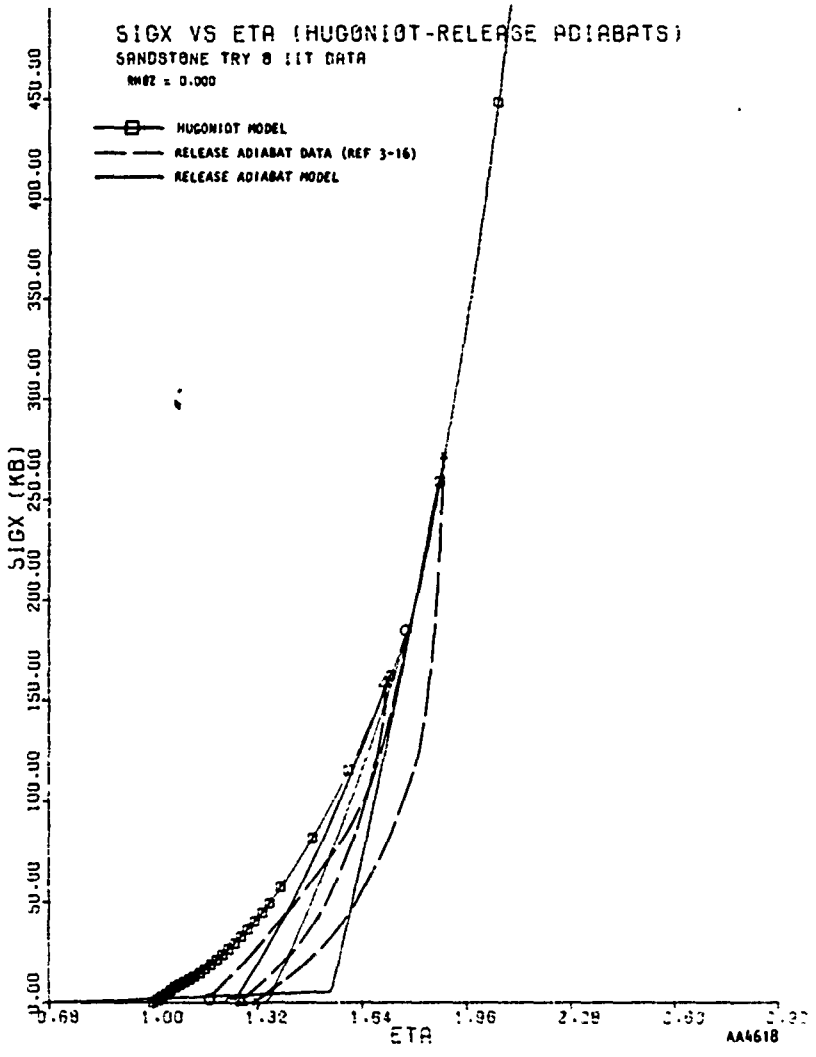

FIGURE 3-10. RELEASE ADIABAT MODEL AND DATA FOR SANDSTONE

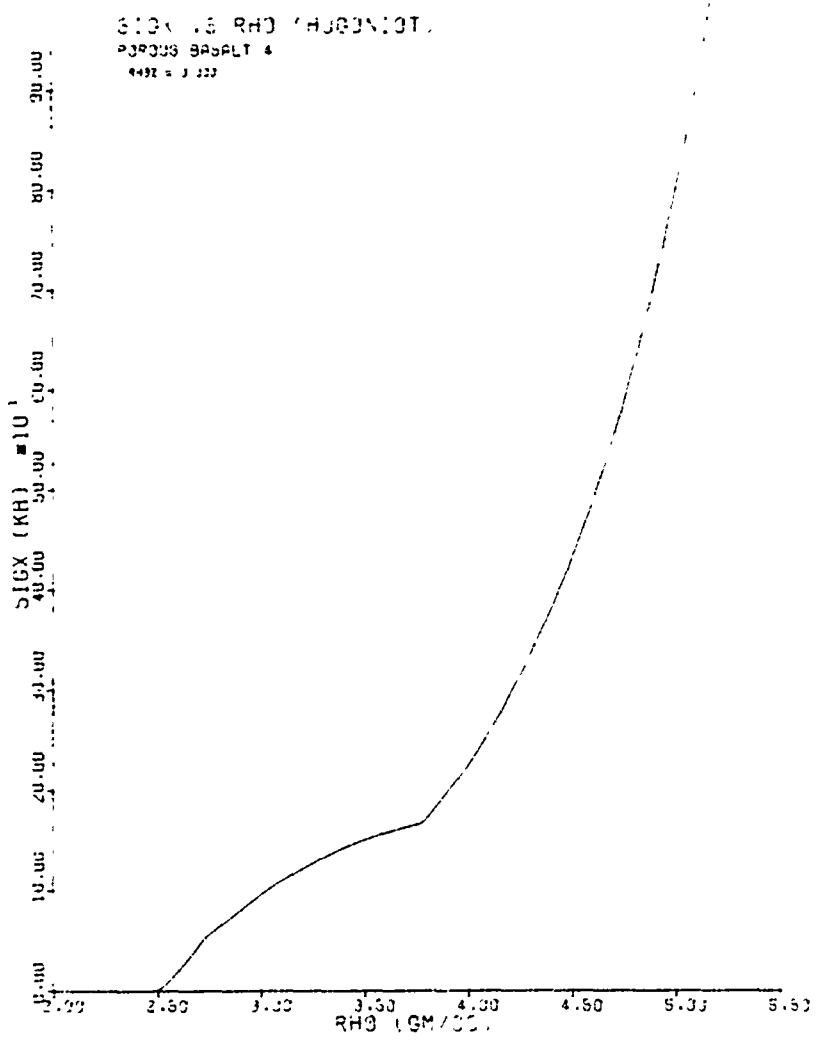

FIGURE 3-11. HUGONIOT MODEL FOR POROUS BASALT

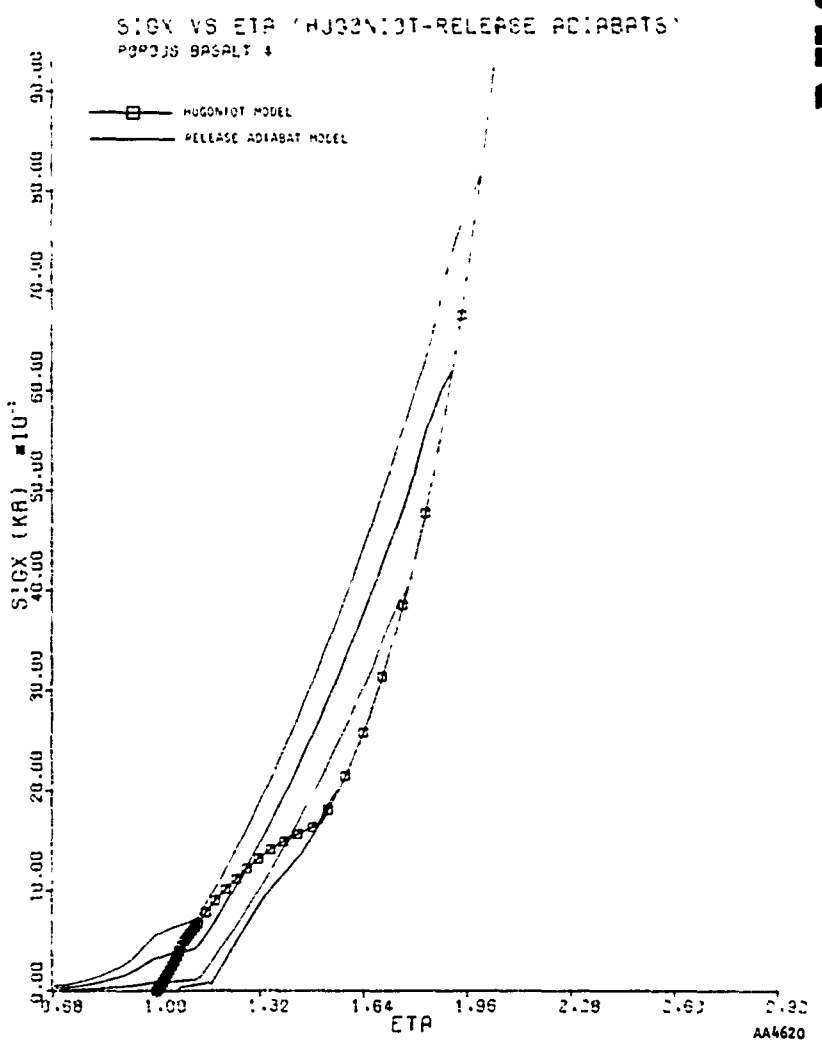

FIGURE 3-12. RELEASE ADIABAT MODEL FOR BASALT

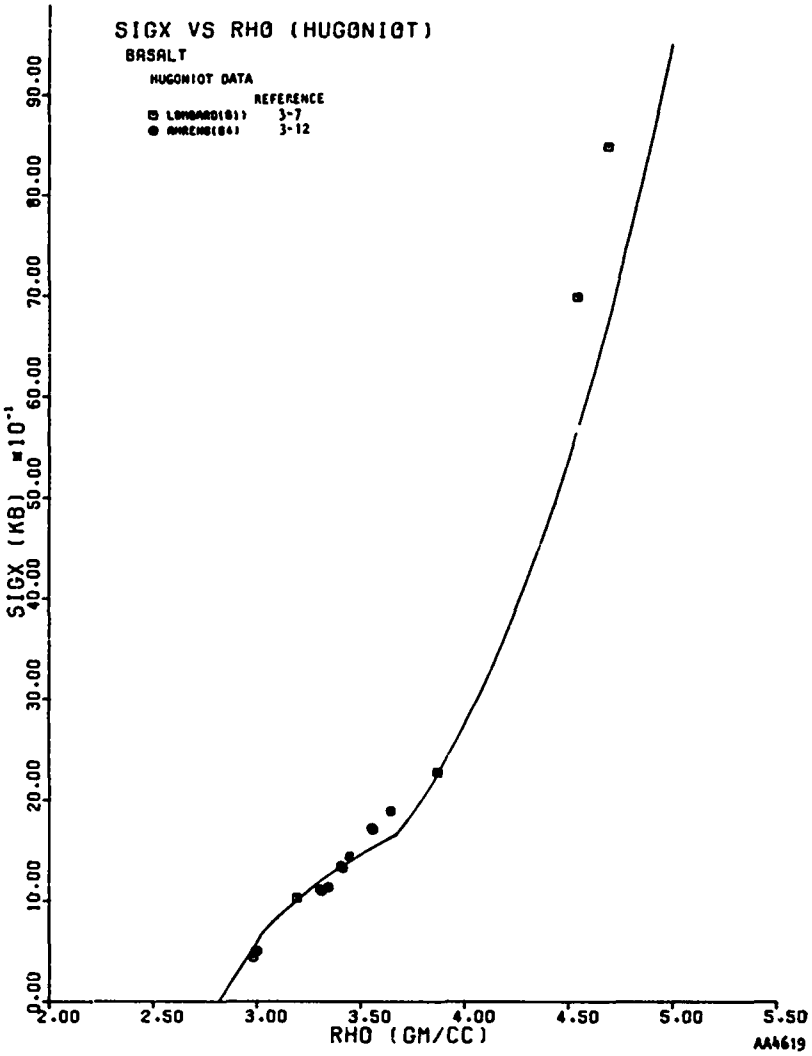

FIGURE 3-13. HUGONIOT DATA AND MODEL FOR DENSE BASALT

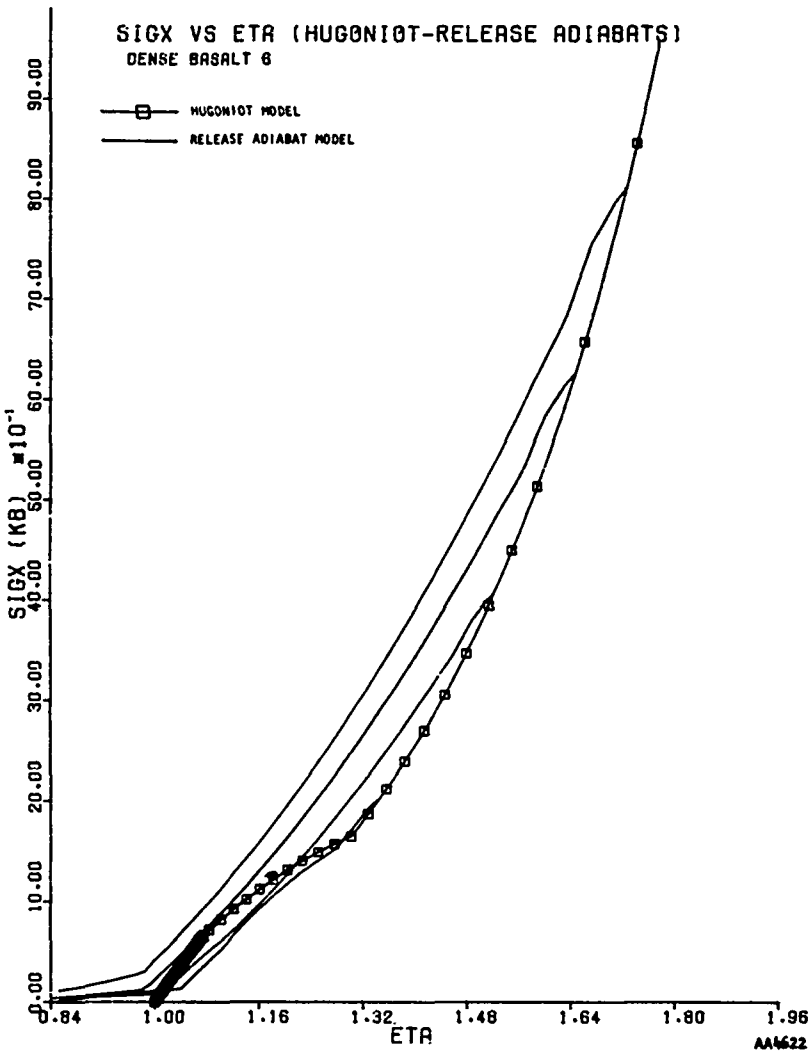

FIGURE 3-14. RELEASE ADIABAT MODEL FOR DENSE BASALT

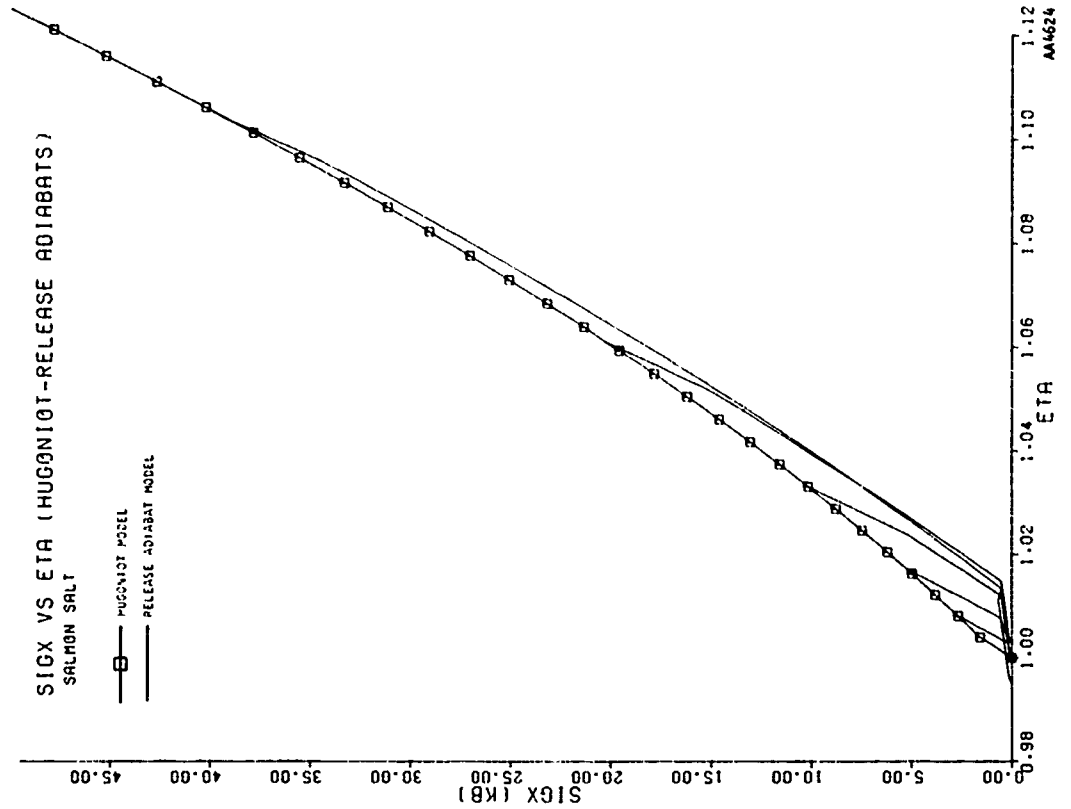

FIGURE 3-16. RELEASE ADIABAT MODEL FOR SALT

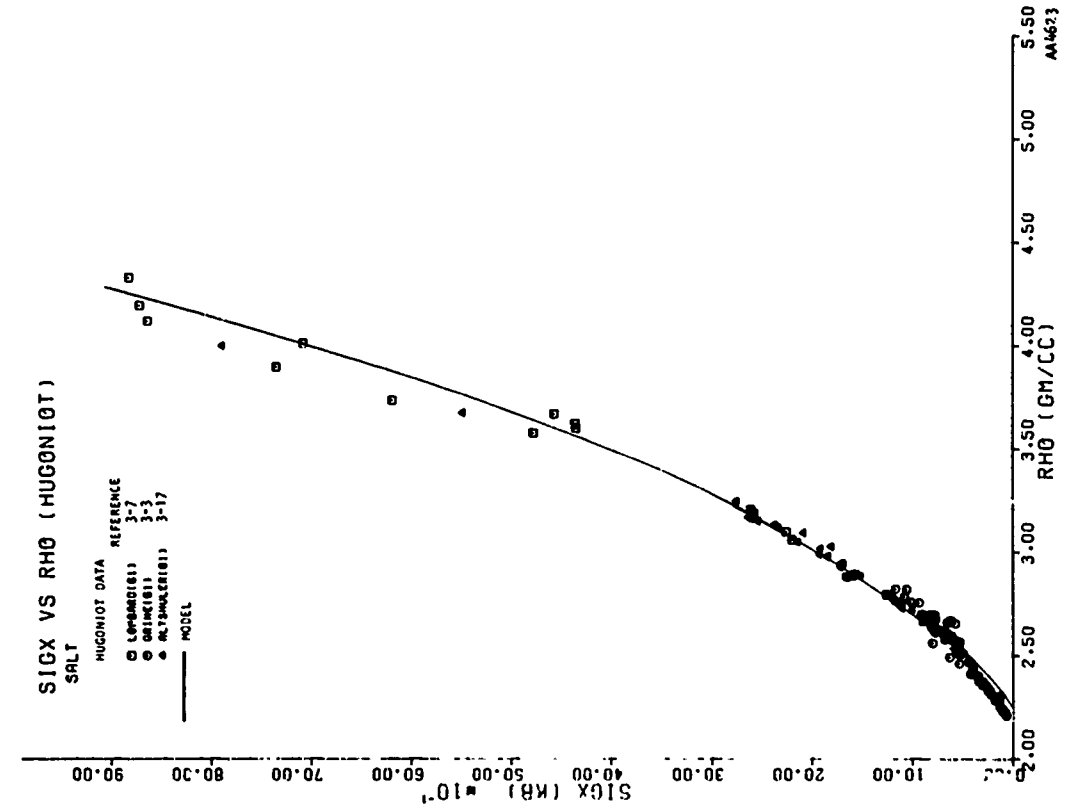

FIGURE 3-15. HUGONIOT DATA AND MODEL FOR SALT

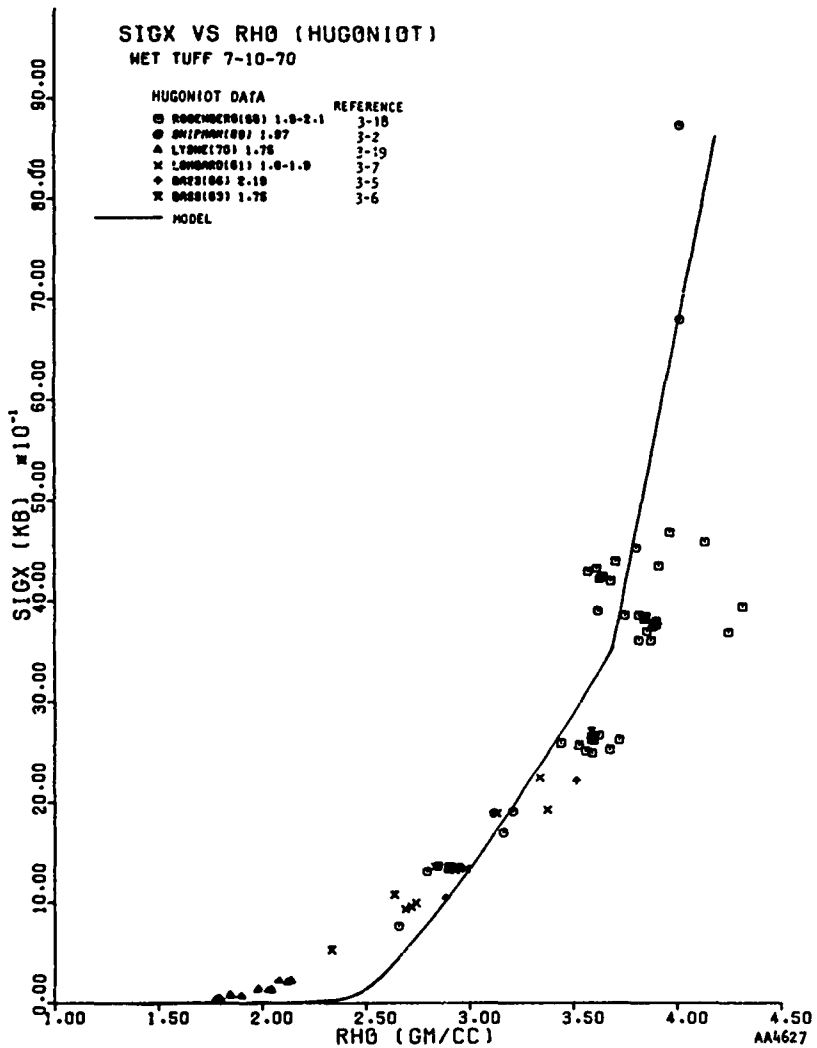

FIGURE 3-17. HUGONIOT DATA AND MODEL FOR WET TUFF

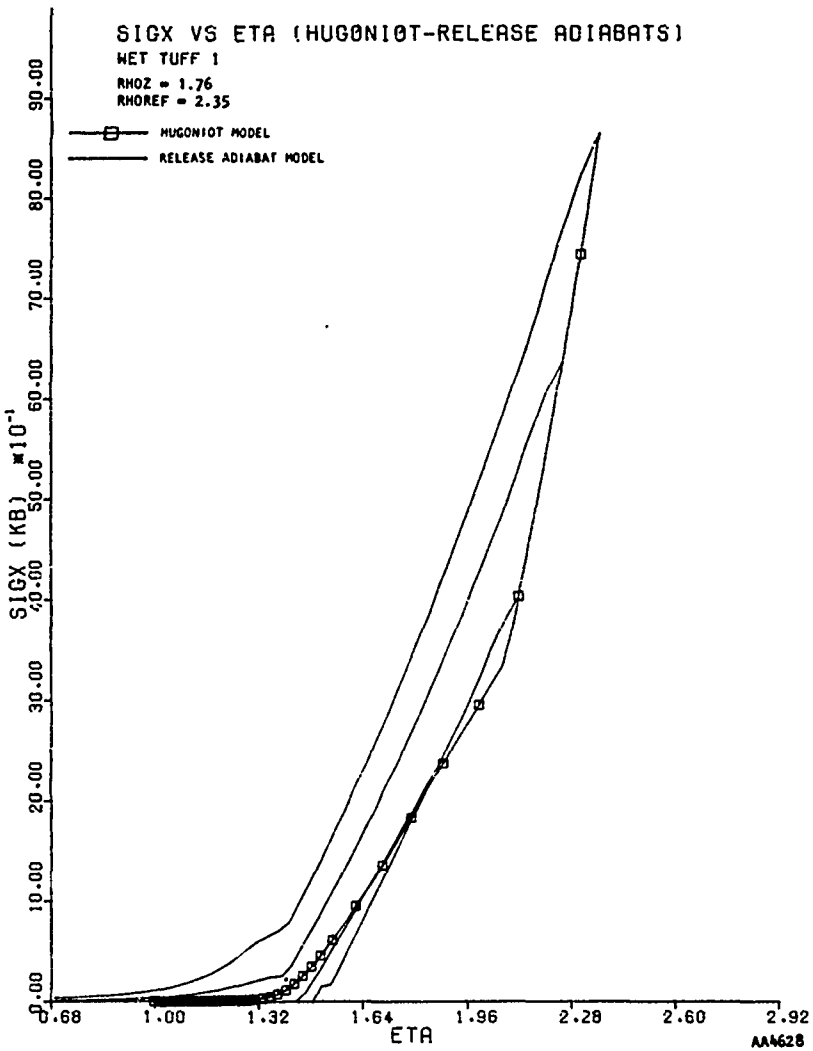

FIGURE 3-18. RELEASE ADIABAT MODEL FOR WET TUFF

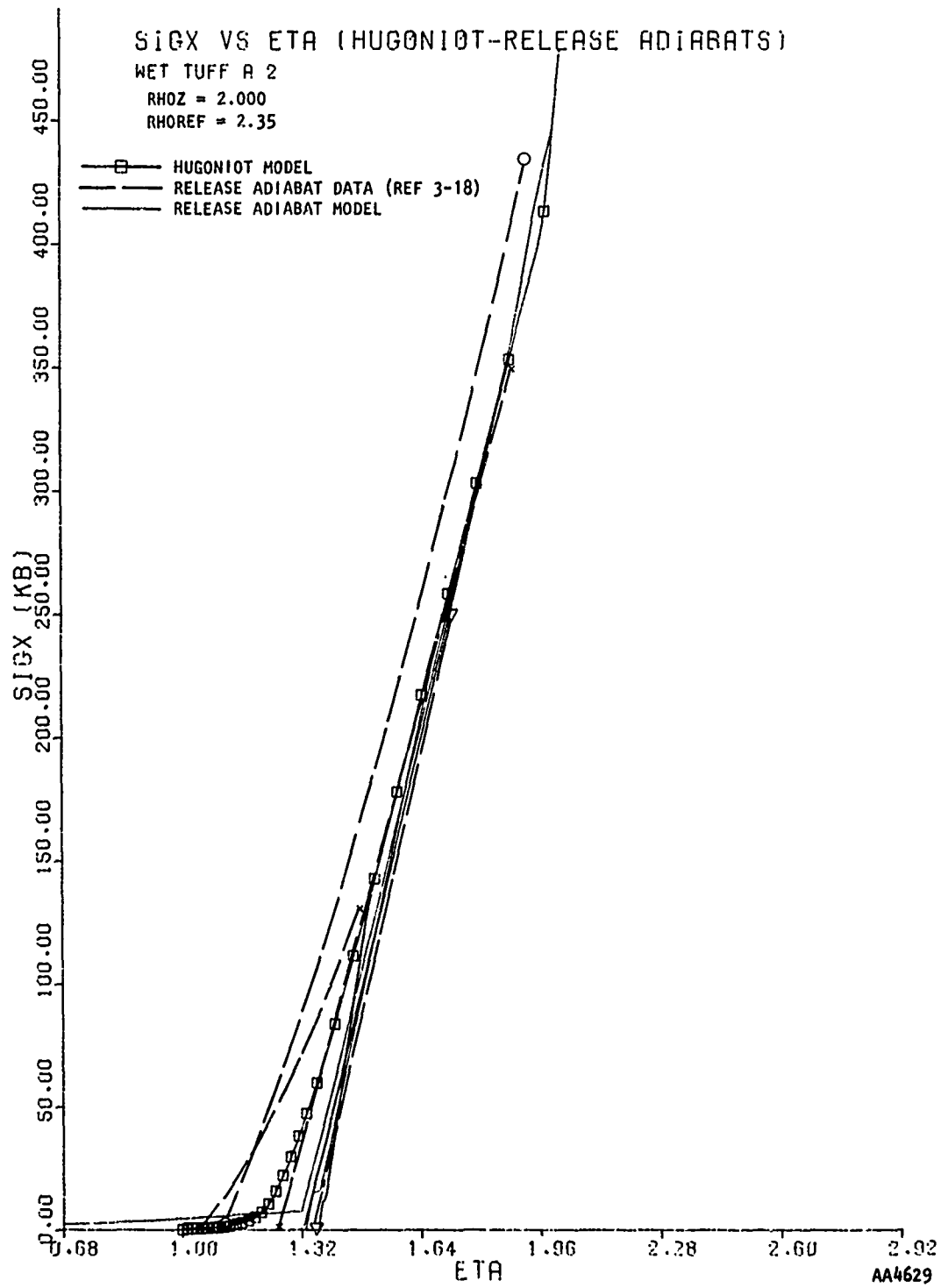

FIGURE 3-19. RELEASE ADIABAT DATA AND MODEL FOR WET TUFF

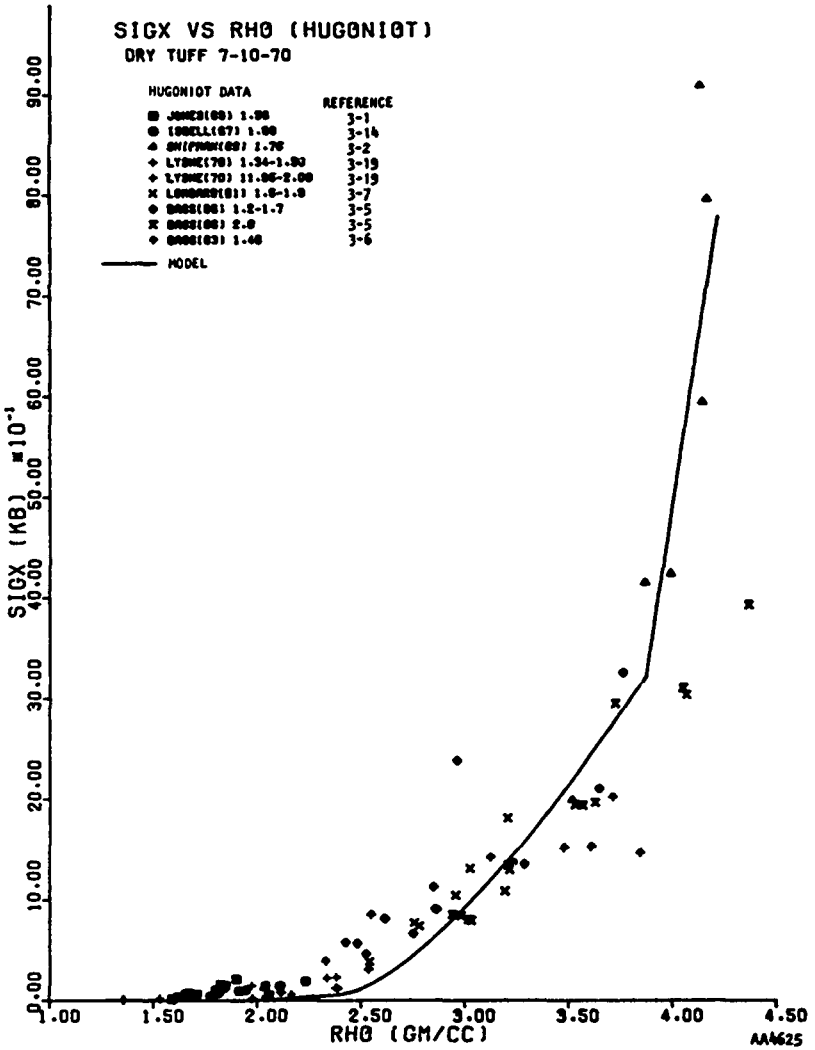

FIGURE 3-20. HUGONIOT DATA AND MODEL FOR DRY TUFF

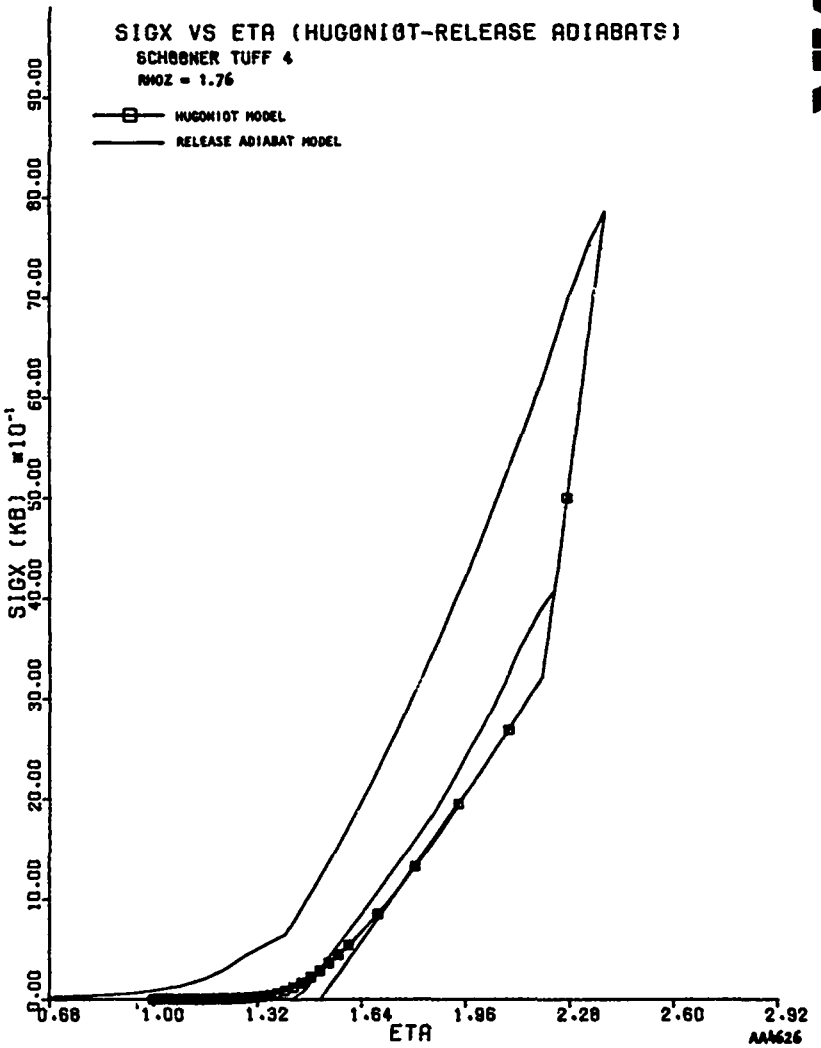

FIGURE 3-21. RELEASE ADIABAT MODEL FOR DRY TUFF

SECTION 4

METHOD OF FITTING THE PRESENT MODEL TO HUGONIOT AND RELEASE ADIABAT DATA

The user of the equations of state presented above may wish to alter the recommended coefficients in order to represent similar materials under different conditions of initial density or moisture content. He may also wish to derive coefficients directly from data for entirely different materials. The following discussion of the model for NTS granite is intended to help the new user do this by indicating how various material parameters are evaluated. Following the discussion of fitting a complete model for NTS granite, some comments on fitting a model to release adiabat data are made.

DERIVATION OF A MODEL FOR NTS GRANITE

The density of granitic rocks may vary from 2.5 to 2.8 gm/cm^3, while samples from the region of interest, Area 15 of the Nevada Test Site (NTS), vary between 2.62 and 2.70 gm/cm^3. Densities are usually determined from measurements on small, competent samples and, hence represent an upper limit to the average density of the rock in a volume comparable to that in the much larger finite difference zones. With this in mind, an initial density of 2.65 gm/cm^3 was selected to represent the granodiorite under consideration.

The calculation of pressure P_s for granite, a solid exhibiting hysteresis, requires the evaluation of nine constants β, K_{max}, K_o, μ^*, c, d, μ_p, μ_{pp}, and P_a. The first, β, is the coefficient of volume expansion per unit internal energy, and can be derived from the ratio of the coefficient of volume expansion per degree Centigrade, and the specific heat. Using values of 25 μin./in. and 0.192 cal/gm (Reference 4-1) for the two above mentioned quantities, $\beta = 3.0$ (cm/cm) $(Mb\text{-}cc/gm)^{-1}$. Although neither the specific heat nor the coefficient of volume expansion is constant over the range of pressure and temperature of interest, both tend to increase linearly with temperature, and it is assumed here that their ratio does not change. A more elaborate representation of β is unwarranted, since βe in Equation 2-5 is usually small relative to the compression unless the material is subjected to pressures on the order of hundreds of kilobars.

The values of K_{max}, K_o, and μ^* for NTS granite can be determined directly from experimental data for pressures below 100 kb. Using a hydrostatic press, Stephens (References 4-2 and 4-3) has obtained loading and unloading pressure/volume data on several NTS rocks for pressures up to 40 kb. In addition, La Mori's measurements (Reference 4-4) of the hydrostats of Westerly granite and tonalite, and Birch's data (Reference 4-5) on the compressional wave speed in various granites prestressed up to 10 kb, provide useful data on possible variations in the hydrostat. Triaxial compression tests, in which all of the stress/strain components have been measured (References 4-6 and 4-7), have been performed at pressures less than 1 kb, and these provide a further check. In an attempt to correlate these experiments, $dP/d\mu$ was calculated from the data reported, and plotted against P. Curves representing the data obtained are compared with the model in Figure 4-1. The variations among the measurements are so large that it is not possible to choose a single value for the "intrinsic" bulk modulus, K_{max}, for all granites. While all of the curves tend toward values between 0.6 and 1.0 Mb, the data vary too much to be fit by a single value of K_{max}. Differences in mineral content are probably responsible for the measured variations in this parameter. A value of 0.8 Mb is chosen as representative of the most recent data on NTS granodiorite (Reference 4-3). Similarly, although K_o ranges between 0 and 0.7 Mb for the variety of granites examined, a value of 0.225 Mb appears appropriate for the NTS material.

The parameter μ^* determines the rate at which the bulk modulus rises from K_o to K_{max}, while the constant c is used to decrease the bulk modulus at high temperatures to match the Hugoniot data in the transition region between solid and fluid. Values of 0.0375 and 0.35 for these two parameters complete the description of the loading hydrostat. In Figure 4-2, calculated hydrostat and Hugoniot curves are compared with data for several granites for pressures in the range 0 to 45 kb. Since the Hugoniot measurements are performed on small samples of highly competent material, most of those data lie above the curve calculated for the in situ material. However, the upper curve, which was calculated by assuming a constant shear modulus appropriate to consolidated granite, fits the data well up to 35 kb. At higher pressures, the measurements on Westerly granite fall below the calculation. This is not unexpected as the bulk modulus, (curve 4a, Figure 4-1), for Westerly granite and, therefore, its hydrostat, are also less than those of NTS granite at these pressures.

The parameters, d, μ_p, μ_{pp}, and P_a are used in describing the unloading behavior of solid material. Walsh (Reference 4-8) has shown that the pressure necessary to close a

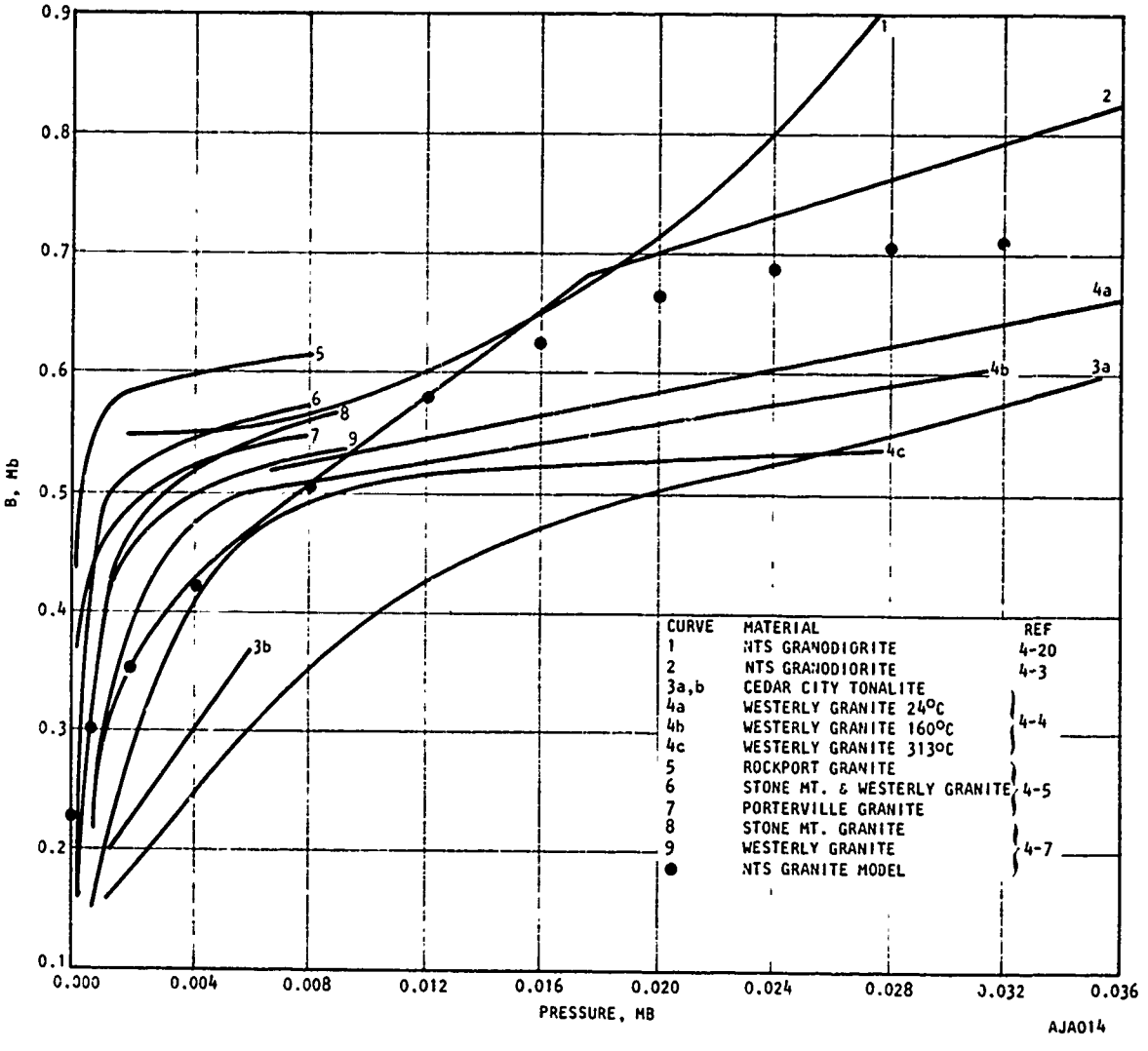

FIGURE 4-1. dP/dμ VERSUS PRESSURE (LOADING) FOR GRANITIC ROCKS

crack is linearly related to the dimensions of the crack. If there are many randomly-sized small cracks which contribute to the initial porosity, it is reasonable to expect an irreversible change in porosity which varies inversly with peak loading pressure until all cracks are closed. No further permanent change in porosity is then exhibited until the pressure is so high that either the pores break down or an irreversible phase change occurs. This behavior is modeled by Equation 2-10, where d is the constant of proportionality between the loss of porosity and the pressure; μ_p is the total change in compression when all the cracks are closed; P_a is the pressure above which pore breakdown and/or phase change is possible; and μ_{pp} is the maximum irreversible change in compression due to pore breakdown or phase change. Unloading paths from the granite Hugoniot are shown in Figure 3-2. At pressures above 400 kb, enough internal energy is present in the material so that the fluid pressure P_f, is not zero. The unloading path from these high pressures drops very sharply until the contribution of P_f to the total pressure dominates. Beyond that point, the pressure diminishes so slowly that the material may not actually return to zero pressure until it has expanded beyond the initial solid density.

Evaluating the parameters for P_f in Equation 2-2 is all that remains to define the behavior of the mean stress in NTS granite. At low densities, the exponential expression, exp Z, damps out everything but the $a_1 \rho e^*$ term. Hence, a_1 is the equivalent of $\gamma - 1$ in the perfect gas law. Calculations at Lawrence Livermore Laboratory (Reference 4-9) show that $\gamma - 1$ asymptotically approaches a value between 0.04 and 0.14 for several rock media at low densities for pressures below 10 kb. Consequently, a_1 was set to 0.1 for all of the rocks modeled in this study. The coefficient α of μ/n in the exponential was set to 5, consistent with the studies on metals by Tillotson (Reference 4-10) and on rocks by Allen (Reference 4-11). For compressed material at energies considerably greater than the vaporization energy, the term

$$\frac{b}{\frac{e}{e_o n^2} + 1}$$

becomes negligible and the coefficient of ρe^* is simply $a_1 + a_2$. The term a_2 was set at 0.4 so that the sum equaled 0.5, again consistent with Tillotson and Allen. This model does differ from Tillotson's formulation in that the term P_f is set to zero at energy densities less than that required to melt the material. For granite, which melts at a temperature of about 1400°C, the minimum energy density for melting, e_{mo}, is assumed to be

0.0115 Mb-cc/gm. Since the melting temperature in most materials increases with compression, the energy density at melting, e_m is allowed to increase linearly to a maximum e_{mm}, equal to 0.035 Mb-cc/gm in granite, so that

$$e_{mo} < e_m = e_{mo}(1 - f\eta) < e_{mm} \qquad (4\text{-}1)$$

where f is set to 1.7. In Figure 3-1 the calculated principal Hugoniot is compared with experimental data up to 1 Mb. Data for several rocks with mineral contents similar to NTS granite are included. Above 100 kb, all of these rocks behave alike, suggesting that their basic chemical composition, rather than initial density, porosity or physical structure, largely determines their behavior at high pressures.

The mean stress behavior of NTS granite is now determined and attention is shifted to the parameters influencing its deviatoric characteristics. Except for Simmons work (Reference 4-2) on the shear wave velocities of rocks under hydrostatic pressures up to 10 kb, there is little data from which to determine the shear modulus, G, of granite. Recently improved techniques in triaxial testing (Reference 4-8) show considerable promise as a means of determining G, but the work is still preliminary. Stephens (Reference 4-13) at Lawrence Livermore Laboratory measured the shear modulus for consolidated and cracked NTS granodiorite. His data, the wave speed measurements of Simmons, and the model are presented in Figure 4-2. The values of G_o, G_{max}, and μ_G^* match Stephens' data for the cracked granodiorite.

Data on the yield strength of granite as a function of mean stress are presented in Figure 4-3. Several Mohr-Coulomb surfaces are also plotted for comparison. The large differences between the various experiments are attributable to the initial condition of the rock, since preexisting cracks and pores or variations in the water content and pore pressure can severely affect the strength of the rock. There is evidence that the yield surface depends to some extent on the stress state (References 4-14 and 4-15), but this is not included in this model. For intact, competent granite, the data is best fit by choosing $k_1 = 0.0005$ Mb and $k_2 = 1.10$. The measurements made on jointed and cracked samples from the Pile Driver site in NTS Area 15 lead to $k_1 = 0.0001$ Mb and $0.5 < k_2 < 0.7$ (References 4-6 and 4-16). Finally, recent unpublished Lawrence Livermore Laboratory data (Reference 4-17) from presumably cracked, wet NTS granite, suggest that k_2 may be as low as 0.3.

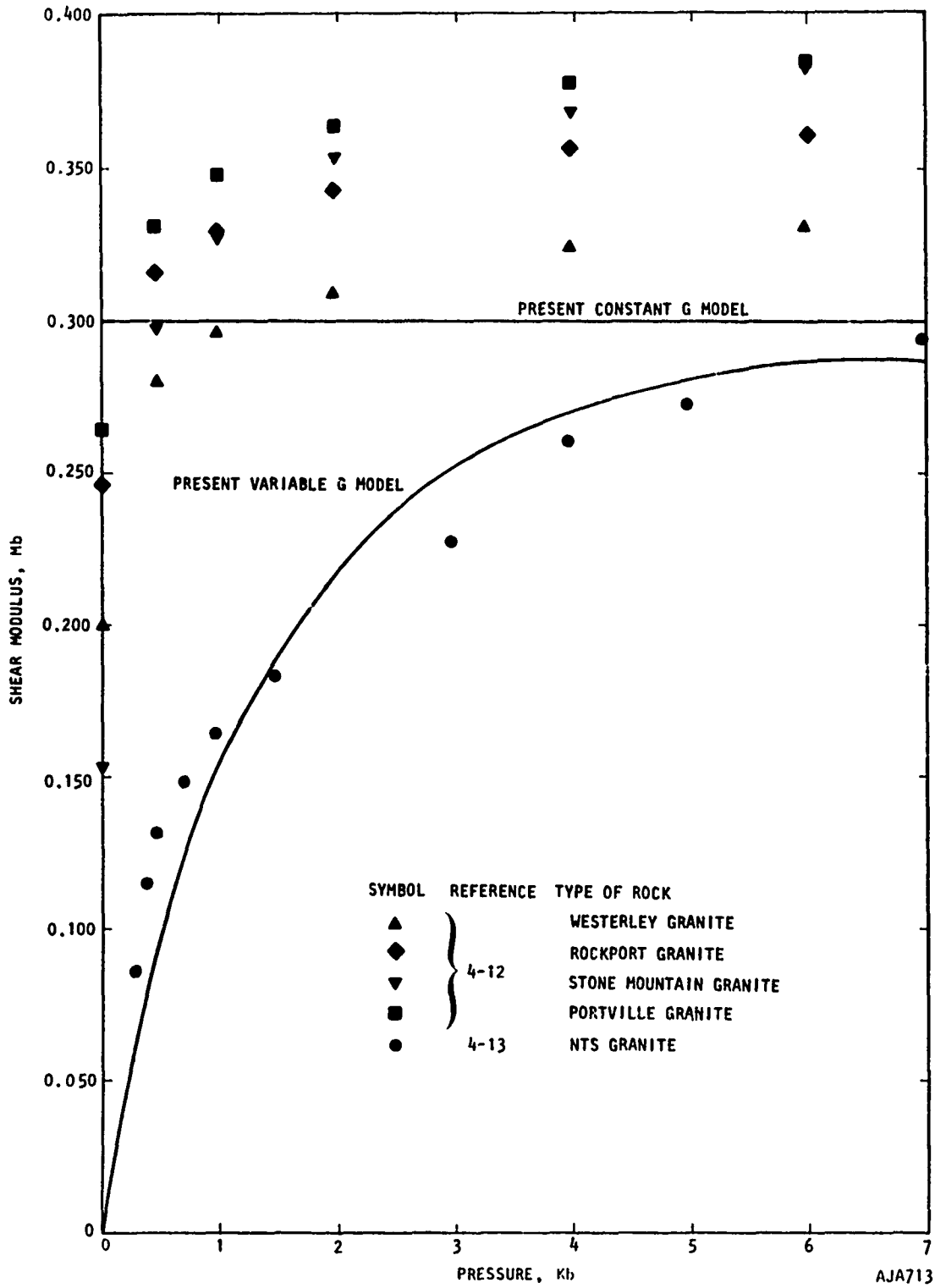

FIGURE 4-2. SHEAR MODULUS VERSUS PRESSURE FOR NTS GRANITE

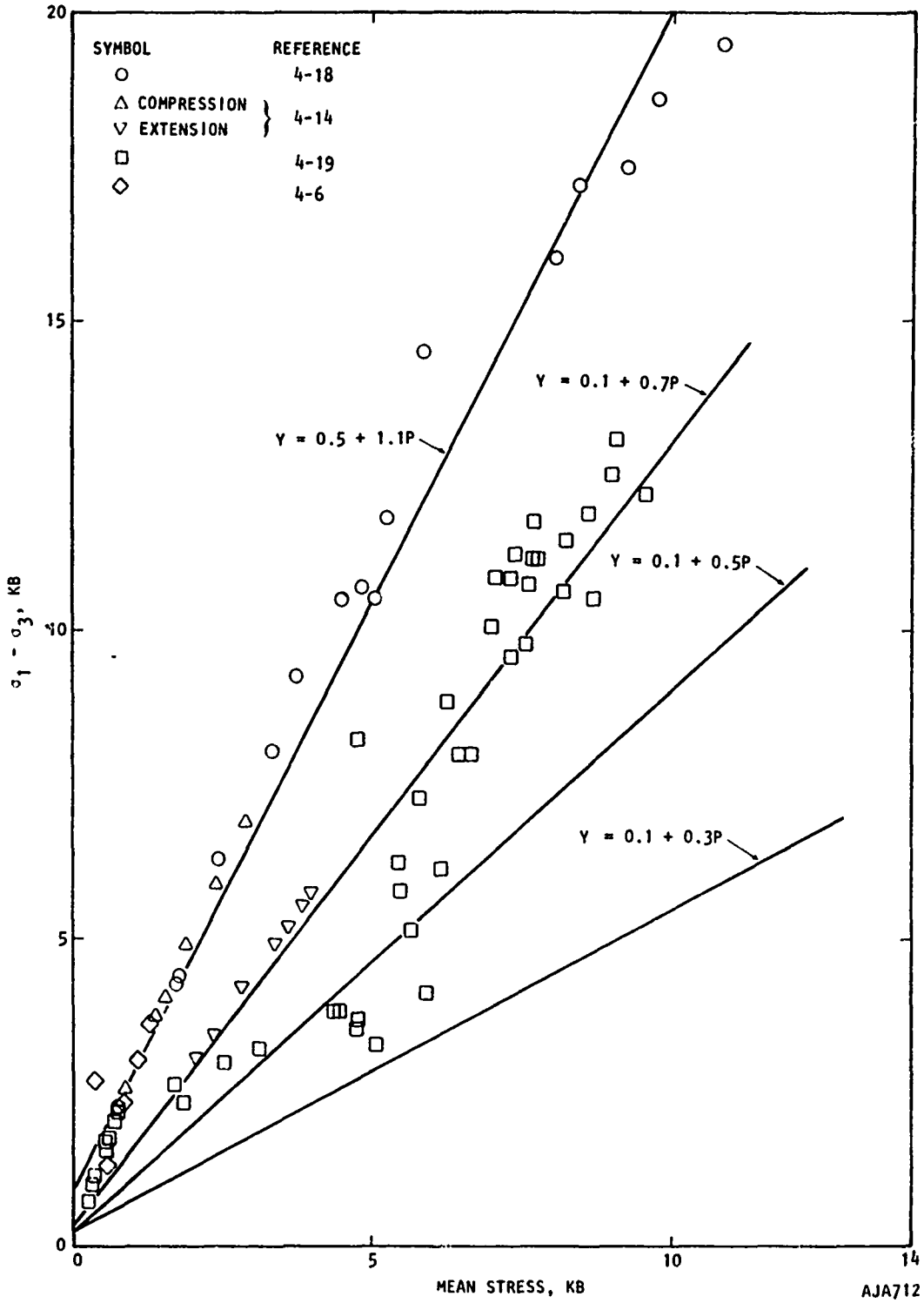

FIGURE 4-3. YIELD STRENGTH VERSUS MEAN STRESS FOR NTS GRANITE

Since the small samples used in the experiments are generally more competent than in situ material, the measured yield strengths have been treated as upper bounds to the values to be expected in the field and values of $k_1 = 0.0001$ Mb and $k_2 = 0.3$ are used in the model. For similar reasons, the von Mises surface, k_3, is set at 0.017 Mb, although comparison of the data near the Hugoniot elastic limit with the calculated hydrostat suggests a value of k_3 as high as 0.020 Mb. The model at low pressure consists chiefly of the hydrostat, shear modulus, yield criterion and flow rule. These are checked by comparing the model hydrostat and hugoniot with the data in Figure 4-4.

APPLICATION OF THE MODEL TO MATCH RELEASE ADIABAT DATA

Fitting the model to release adiabat data is performed by selecting the parameters μ, P_a, μ_{pp}, e_{mo}, and f.

The amount of hysteresis which occurs before melting, that is when

$$e \leq e_m$$

is controlled through the parameters μ_p, μ_{pp}, P_a, and d as indicated in Equation 2-10. Increasing μ_p and μ_{pp} increases the amount of hysteresis and the slope of the release adiabat.

Behavior such as that shown in Figure 4-5 is controlled through the parameters e_{mo} and f. By raising e_{mo} or f, the energy required to vaporize the solid is raised and the solid material remains a solid (Case 2). By lowering e_{mo} or f, the energy required to vaporize the solid is decreased and the pressure may still be governed appreciably by the gas contribution; in this case when the pressure gets low enough, expansion beyond the initial volume can occur (Case 1).

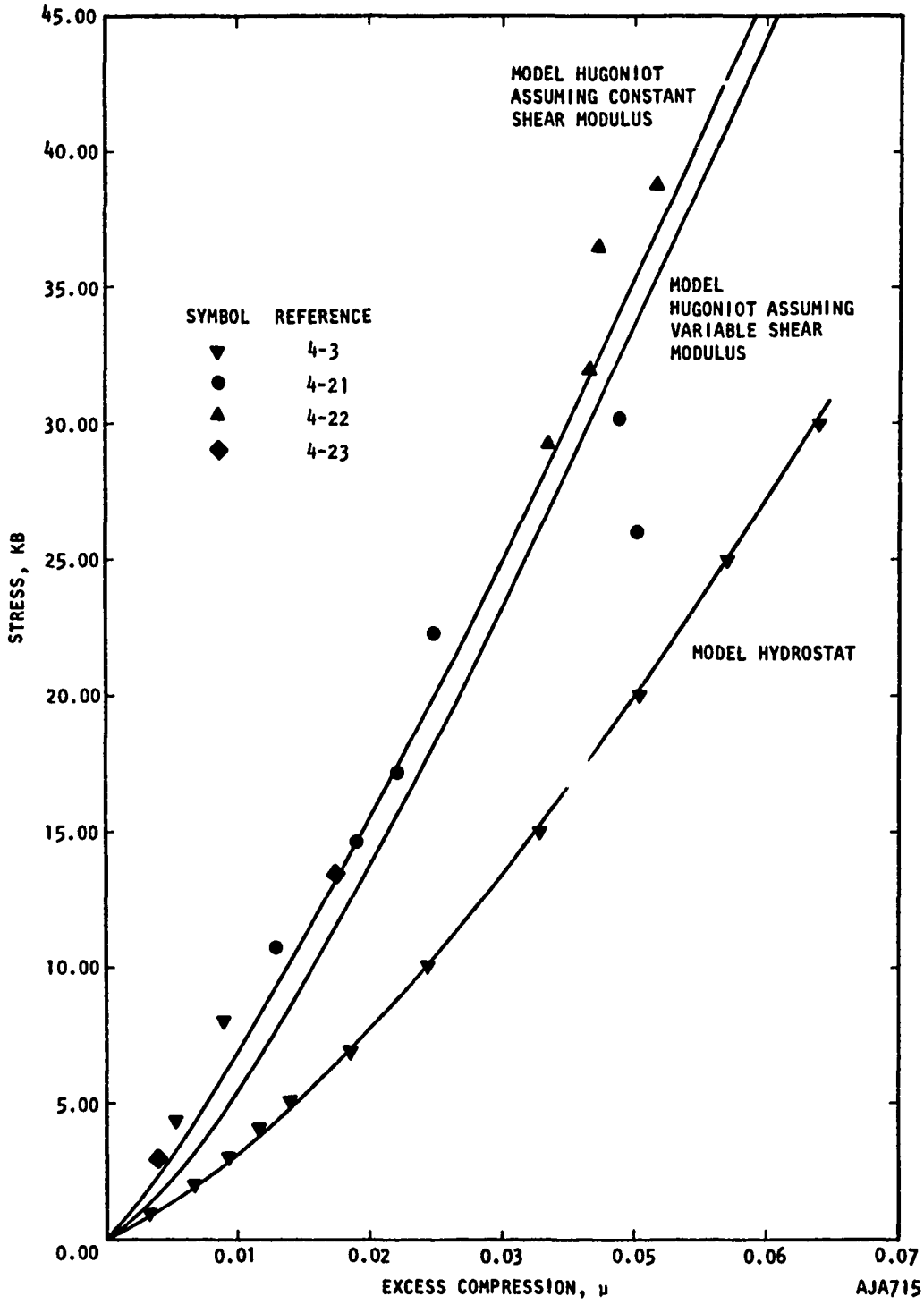

FIGURE 4-4. MODEL HUGONIOT AND HYDROSTAT FOR NTS GRANITE COMPARED WITH DATA

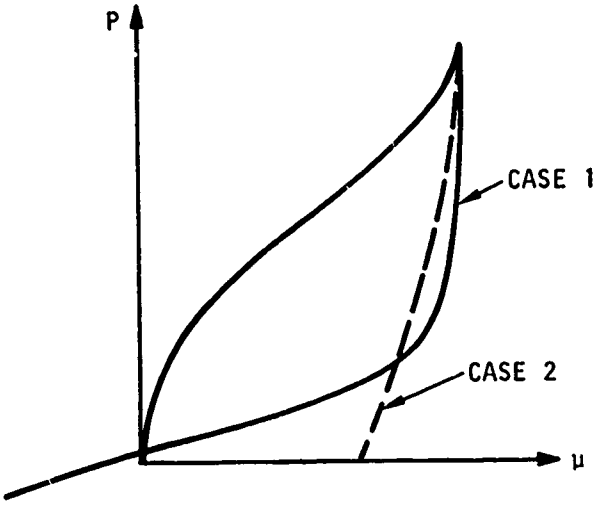

IN CASE 1, THE VALUE OF e AT P = 0 IS GREATER THAN $e_{mo}(1 + f\mu_{max})$

IN CASE 2, THE VALUE OF e AT P = 0 IS LESS THAN $e_{mc}(1 + f\mu_{max})$

FIGURE 4-5. MODEL RELEASE ADIABATS

REFERENCES

4-1. *Handbook of Chemistry and Physics*, Chemical Rubber Publishing Company, 36th Ed., 1955, pp. 2061-2103.

4-2. Stephens, D. R., and E. M. Lilley, *Static PV Curves of Cracked and Consolidated Earth Materials to 40 Kilobars*, UCRL-14711, Lawrence Radiation Laboratory, March 1966.

4-3. Private communication from D. R. Stephens (Lawrence Radiation Laboratory), 1968.

4-4. LaMori, P. N., *Compressibility of Three Rocks, (A) Westerly Granite and Solenhofen Limestone to 40 Kilobars at 300°C, (B) Cedar City Tonalite to 40 Kilobars at Room Temperature*, DASA-2151, Defense Atomic Support Agency, August 1968.

4-5. Birch, F., "Velocity of Compressional Waves in Rocks to 70 Kilobars, Part 1," *J. Geophys. Res.*, Vol. 65, No. 4, 1960, p. 1083.

4-6. *Tests for Strength Characteristics of Rock, Pile Driver Project*, MRDL 64/90, U. S. Army Corps of Engineers, Missouri River Division Laboratory, 1964.

4-7. Brace, W. F., "Some New Measurements of Linear Compressibility in Rocks," *J. Geophys. Res.*, Vol. 70, No. 2, 1965, p. 391.

4-8. Walsh, J. B., "The Effect of Cracks on the Compressibility of Rock," *J. Geophys. Res.*, Vol. 70, No. 2, January 15, 1965.

4-9. Butkovitch, T. R., *The Gas Equation of State for Natural Materials*, UCRL-14729, Lawrence Radiation Laboratory, January 1967.

4-10. Tillotson, J., *Metallic Equations of State for Hypervelocity Impact*, GA-3216, General Atomic Div., General Dynamics Corporation, July 1962.

4-11. Allen, R. T., *Equation of State of Rocks and Minerals*, GAMD-7834, General Atomic Div., General Dynamics Corporation, 1967.

4-12. Simmons, G., "Velocity of Shear Waves in Rocks to 10 Kilobars, Part 1," *J. Geophys. Res.*, Vol. 69, No. 6, 1964, p. 1123.

4-13. Stephens, D. R., *Elastic Constants of Fractured Granodiorite*, UCID-15369, Lawrence Radiation Laboratory (to be published).

4-14. Mogi, K., "Effect of the Intermediate Principal Stress on Rock Failure," *J. Geophys. Res.*, Vol. 72, No. 20, October 1967, p. 5117.

4-15. Brown, W. S., et al., *Influence of Dynamic Loading, Biaxial Loading and Prefracturing on the Stress-Strain and Fracture Characteristics of Rocks*, DASA-2713, University of Utah, March 1971.

4-16. Byerlee, J. D., "Frictional Characteristics of Granite Under High Confining Pressure," *J. Geophys. Res.*, Vol. 72, No. 14, 1967, p. 3639.

4-17. Private communication from H. Heard (Lawrence Radiation Laboratory) via D. R. Stephens (Lawrence Radiation Laboratory), 1968.

4-18. Brace, W. F., et al., "Dilatency in the Fracture of Crystalline Rocks," *J. Geophys. Res.*, Vol. 71, No. 16, August 15, 1966.

4-19. Giardini, A. A., et al., "Triaxial Compression Data on Nuclear Explosion Shocked, Mechanically Shocked and Normal Granodiorite from the Nevada Test Site," *J. Geophys. Res.*, Vol. 73, No. 4, February 15, 1968, p. 305.

4-20. Stephens, D. R., and E. M. Lilley, *Static PV Curves of Cracked and Consolidated Earth Materials to 40 Kilobars*, UCRL-14711, Lawrence Radiation Laboratory.

4-21. Jones, A. H., and N. H. Froula, *Uniaxial Strain Behavior of Four Geological Materials to 50 Kilobars*, DASA-2209, March 1969.

4-22. Grine, D. R., *Equations of State of Granite and Salt*, UCRL-13004, Lawrence Radiation Laboratory, May 1961.

4-23. Ainsworth, D. L., and B. R. Sullivan, *Shock Response of Rock at Pressures Below 30 Kilobars*, WES TR 6-802, U. S. Army Engineer Waterways Experiment Station, November 1967.

APPENDIX A

During the course of fitting and checking the models described above, references containing release adiabat data were found. These references, some of which themselves contain extensive lists of references, are given below.

TABLE A-1.

Material	Pressure Range, k Bar	Reference
Alluvium, Frenchman's Flat, NTS	1 to 12	A-9
Playa, Area 5, NTS, 0 to 18.9% Moisture	70 to 280	A-2
Tuff, Area 12, NTS, dry	85 to 125	A-4
Tuff, Area 19, NTS, dry	20 to 290	A-8
Tuff, Area 12, NTS, saturated	115 to 145	A-4
Tuff, Rainier Mesa, NTS, saturated	135 to 470	A-6
Sandstone, Coconino, dry	155 to 255	A-4
Quartz, Arkansas Novaculite	70 to 150	A-1
Quartz, Arkansas Novaculite	70 to 380	A-3
Quartz, Fused Glass	100 to 380	A-6
Granite, Raymond, California	45 to 285	A-5
Granodiorite, Climax Stock, NTS	190 to 285	A-8
Tonalite, Cedar City, Utah	10 to 65	A-9
Anorthosite, San Gabriel Mtns., Calif.	55 to 422	A-3
Alluvium	80 to 285	A-11

REFERENCES

A-1. Ahrens, T. J., et al., *Dynamic Properties of Rocks*, Interim Report, DASA-1694, SRI, April 1965.

A-2. Anderson, G. D., et al., *Investigation of Equation of State of Porous Earth Media*, AFWL-TR-65-146, SRI, February 1966.

A-3. Ahrens, T. J., et al., *Dynamic Properties of Rocks*, DASA-1868, SRI, September 1966.

A-4. Wiedermann, A. H., et al., *Shock Unloading Characteristics of Porous Geological Materials*, AFWL-TR-66-118, IIT Res. Inst., January 1967.

A-5. Keough, D. D., et al., *Piezoresistive Stress-Time Transducer Development and Granite Adiabat Measurements for Project Pile Driver*, DASA-2131, SRI, February 1967.

A-6. Rosenberg, J. T., et al., *Dynamic Properties of Rocks*, DASA-2112, SRI, July 1968.

A-7. Shipman, F. H., et al., *High Pressure Hugoniot Measurements for Several Nevada Test Site Rocks*, DASA-2214, General Motors Corporation, March 1969.

A-8. Petersen, C. F., *Shock Wave Studies of Selected Rocks*, Ph. D. Thesis, Stanford University, May 1969.

A-9. Petersen, C. F., et al., *Dynamic Properties of Rocks*, DASA-2298, SRI, June 1969.

A-10. Ahrens, T. J., *Evaluation of Equation of State Data*, DASA-2359, California Institute of Technology, January 1970.

A-11. Murri, W. J., and C. W. Smith, *Equation of State of Rocks*, Stanford Research Institute, Interim Technical Report to USAEC, March 31, 1970.